Acta Biomaterialia xxx (xxxx) xxx

Contents lists available at ScienceDirect

Acta Biomaterialia

journal homepage: www.elsevier.com/locate/actbio

Full length article

Mechanical characterization of infarcted porcine hearts using left anterior descending and left circumflex coronary artery models

Nicolás Laita [a,b,*], Alejandro Aparici-Gil [a,c], Aida Oliván-Viguera [a,c,d], Alba Pérez-Martínez [a,c,d], Ming Wu [e], Manuel García de Yébenes [f], Gloria Abizanda [g], Stephan Janssens [e], Felipe Prósper [h,i,j,k], Manuel M. Mazo Vega [g,h,i], Miguel Ángel Martínez [a,c], Manuel Doblaré [a,c,d,l], Estefanía Peña [a,c]

[a] Aragon Institute of Engineering Research (I3A), University of Zaragoza, Spain
[b] Instituto Tecnologico de Aragon (ITA), Zaragoza, Spain
[c] Centro de Investigacion Biomedica en Red en Bioingenieria, Biomateriales y Nanomedicina (CIBER-BBN), Spain
[d] Aragon Institute of Health Research (IIS Aragon), Spain
[e] Department of Cardiovascular Sciences, University of Leuven, Belgium
[f] Department of Cardiology, Clinica Universidad de Navarra, Pamplona, Spain
[g] Biomedical Engineering Program, Enabling Technologies Division, CIMA Universidad de Navarra, Pamplona, Spain
[h] Hematology and Cell Therapy, Clinica Universidad de Navarra, Pamplona, Spain
[i] Instituto de Investigacion Sanitaria de Navarra (IdiSNA), Pamplona, Spain
[j] Hemato-Oncology Program, Cancer Division, CIMA Universidad de Navarra, Pamplona, Spain
[k] Centro de Investigacion Biomedica en Red en Cancer (CIBERONC team CB16-12-00489), Pamplona, Spain
[l] Nanjing Tech University, China

ARTICLE INFO

Keywords:
Porcine cardiac tissue
Myocardial infarction
Left descendant artery infarction model
Left circumflex artery infarction model
Experimental characterization
In vitro testing
Biaxial
Simple triaxial shear
Confined compression
Tissue engineering

ABSTRACT

This study comprehensively analyzes passive mechanical and structural changes of cardiac tissue 6 weeks after myocardial infarction (MI) by biaxial, simple triaxial shear, and confined compression characterization. We considered a porcine model, comparing two MI types: Left Anterior Descending (LAD) artery and Left Circumflex (LCX) artery occlusions. LAD model generated apical transmurally infarcted hearts, while the LCX model generated medial heterogeneous infarctions ranging from mild locally infarcted tissue to transmurally infarcted tissue. Infarcted tissue exhibited significantly higher stiffness than healthy tissue. When peak equibiaxial stretch increases up to 20%, the stress increase is 2.19 for medial locally infarcted tissue, 4.49 for medial fully infarcted tissue, and 6.26 for apical fully infarcted tissue. Fully infarcted animals showed significant macroscopic geometrical remodeling, with thickness reductions in the infarcted area of 45%–60%, while locally infarcted tissue showed no thinning. The anisotropy of healthy myocardium was also altered post-MI: medial infarcts exhibited preferentially circumferential anisotropy, while apical infarctions increased isotropy. Histological analysis validated these mechanical alterations, revealing a substantial increase in collagen content in infarcted regions. In LCX infarctions, collagen distribution was uniformly aligned, whereas in LAD ones, its distribution was spatially heterogeneous. Non-infarcted tissue far from the infarction did not exhibit changes in mechanical properties or collagen content, suggesting a localized effect at least 6 weeks post-MI. These findings highlight the importance of considering the extent and location of MI when developing personalized therapeutic strategies.

Statement of Significance

This work provides a comprehensive mechanical and histological assessment of post-infarct porcine myocardium using advanced multimodal testing. Unlike previous studies, we compare two infarct types (LAD and LCX) under identical conditions and examine regional and severity-dependent differences in stiffness, compressibility, and anisotropy. We show that infarction induces local rather than global changes in tissue passive mechanics, modulated by infarct geometry and scar distribution. These insights support more accurate cardiac modeling and may guide personalized therapeutic strategies after myocardial infarction.

* Corresponding author at: Aragon Institute of Engineering Research (I3A), University of Zaragoza, Spain.
E-mail address: nlaita@unizar.es (N. Laita).

https://doi.org/10.1016/j.actbio.2025.12.051
Received 11 June 2025; Received in revised form 26 December 2025; Accepted 30 December 2025
Available online 5 January 2026

1. Introduction

Myocardial infarction (MI) remains one of the leading causes of death worldwide. It involves the necrosis of cardiac tissue due to prolonged hypoxia, caused by the occlusion of a coronary artery. Myocardial tissue exhibits a complex architecture and mechanical behavior, typically described through two components: an active response, linked to autonomous contraction, and a passive response, governed by its microstructural organization. Focusing on the latter, LeGrice et al. [1] identified a characteristic three-dimensional arrangement in the left ventricular (LV) myocardium, the most common site of MI, with three principal axes: muscle fibers (f), sheet direction (s), and normal to the cleavage planes (n). This '*FSN*' structure results in locally orthotropic mechanics. Several studies have explored the full 3D response of the myocardium using protocols such as biaxial extension, simple shear, and pure shear [2–6]. Others have examined myocardial compressibility [6–10], a feature often neglected in computational models, despite evidence of its relevance in simulating cardiac mechanics [11,12].

These baseline properties, however, are profoundly altered following MI. Beyond the immediate loss of contractile function within minutes of ischemia, the infarcted region undergoes a progressive and drastic remodeling. Holmes et al. [13] described this process in four phases: acute ischemia, necrosis, fibrosis, and remodeling. These stages span weeks to months, depending on the species [14]. In large-animal models, such as the pig, the main remodeling phase lasts around six weeks [13]. Each phase presents distinct mechanical profiles [13,14]: (i) during acute ischemia (first hours), passive properties remain near-physiological; (ii) in the necrotic phase (5–7 days), tissue may soften due to collagen/titin degradation or stiffen from edema, with edema typically dominating; (iii) during fibrosis (2–4 weeks), stiffness increases due to a dense collagen deposition; and (iv) in late remodeling (the remainder of the healing process), collagen cross-linking governs mechanical behavior.

However, several factors modulate these trends. Infarct size is a major predictor of dysfunction. Larger infarcts associate with worse outcomes [15,16], with risk increasing sharply beyond 40%–50% LV involvement, while <35% scarring rarely leads to cardiogenic shock [17]. Total scar volume, rather than infarct number, appears to dictate prognosis. Additionally, infarct location influences tissue mechanics, as highlighted in Fomovsky et al. [18], who related collagen alignment with different ventricular locations and their respective regional anisotropy. Lastly, while collagen content, orientation, and cross-linking are considered key determinants of scar mechanics [18–20], especially during late remodeling, their precise roles remain under debate [20,21].

This complex mechanical behavior of infarcted myocardium has motivated numerous studies to characterize its evolving properties using both *in vitro* and *in vivo* approaches. Early *in vitro* efforts were conducted by Gupta et al. [21], who performed equibiaxial testing on infarcted ovine tissue. MI was induced in the anteroapical region, and samples were taken near the anteromedial zone. They observed notable changes in stiffness and anisotropy throughout the healing process, while remote (non-infarcted) tissue maintained stable mechanical properties. These findings were later validated via simulations by McGarvey et al. [22]. Fomovsky et al. [20] also performed equibiaxial tests on apical infarcted murine hearts at various post-MI time points (1, 2, 3, and 6 weeks). They reported progressive stiffening proportional to collagen accumulation and an overall isotropic mechanical response in the scar. Zhang et al. [23] extended this approach to porcine hearts, comparing infarcted samples from anteromedial, anteroapical, and posteromedial regions. Their results showed isotropic behavior in apical infarcts and increased anisotropy in both medial zones. Similarly, Morita et al. [24] found isotropic behavior in ovine apical infarcts, in line with Fomovsky's findings. This methodology was further expanded by Martonová et al. [25]. Sirry et al. [26,27] extended the existing protocols by introducing non-equibiaxial and compressive tests on medial infarcted murine tissue at 0, 1, 2, and 4 weeks post-MI. They confirmed the progressive stiffening and anisotropy observed in earlier studies, and demonstrated increased incompressibility and in-plane coupling over time. To the best of our knowledge, this remains the only procedure that has evaluated infarct tissue compressibility directly. Avazmohammadi et al. [5] also investigated apical infarcted ovine tissue under biaxial and triaxial loading. While their primary goal was to validate their testing methodology, the observed mechanical trends were consistent with those of Morita [24]. Finally, the recent study by Mendiola et al. [28] introduced a novel *in vitro* microstructural analysis that integrates histological data on muscle and collagen fiber orientation. A summary of the existing experimental protocols is provided in Table 1.

Regarding *in vivo* studies, Holmes et al. [19] measured radial, longitudinal, and circumferential strains in medial infarcted porcine tissue using gold markers. They found a notable reduction in circumferential strain, suggesting increased stiffness in that direction, likely due to the collagen accumulation observed histologically. Fomovsky et al. [18] expanded on this by comparing infarcts of different shapes and locations (apical vs. medial) in murine hearts. Apical infarcts showed random collagen networks and isotropic behavior, while medial infarcts displayed circumferential alignment and anisotropic response. They concluded that the pre-MI strain environment shapes the structural organization of the scar, a finding supported by previous studies [19–21,24,26] and earlier suggested by Zimmerman [29], who showed that modifying tissue mechanics alters its structure and function. Similar patterns were also reported by Zhang [23]. More recently, *in vivo* research has shifted towards computational models that estimate infarct properties indirectly, either to predict post-MI mechanics [30–32] or to support therapeutic development [33]. These models often assume infarcted tissue behaves like healthy myocardium scaled by a stiffening factor. Despite their simplifications, they have shown adequate accuracy for their objectives [34,35].

As shown, numerous studies have examined the mechanical evolution of infarcted myocardium. However, several key questions remain unanswered. Most *in vitro* studies, except Zhang's [23], focus on a single infarct location or model, without comparing different MI types under the same controlled conditions, as was done *in vivo* by Fomovsky et al. [18]. In addition, most works are limited to equibiaxial testing, with only a few exceptions such as the studies by Sirry [26] and Mendiola [28]. This limitation also applies to the characterization of tissue compressibility, which, as in healthy myocardium, remains poorly explored post-MI. Although Sirry already reported variations in compressibility [26], this property has not received sufficient attention. Recent works have shown that myocardial compressibility may significantly affect the accuracy of cardiac simulations [11,12]. Finally, except for the early studies of Gupta et al. [21], most studies focus exclusively on infarcted regions, while the mechanical response of adjacent or remote myocardium remains largely undercharacterized.

For all these reasons, this study aims to provide new insights into the post-MI state by conducting an *in vitro* multimodal experimental characterization, including biaxial, triaxial shear, and confined compression tests to evaluate stiffness and anisotropy in infarcted tissue. These tests were complemented with histological analyses to examine changes in muscle fiber alignment and collagen distribution. Using a porcine model, we compared two frequent infarction types induced by occlusion of the Left Anterior Descending (LAD) and Left Circumflex (LCx) arteries to explore how infarct location influences remodeling. Our objectives were: (i) to directly assess the mechanical response of distinct infarct models, expanding on Fomovsky's findings [18]; (ii) to compare infarcted, proximal and remote tissue under multiple loading conditions, quantifying the spatial extent of MI effects; and (iii) to characterize compressibility in both infarcted and remote regions, following the limited prior data available from Sirry et al. [26]. Furthermore, (iv) we examined varying infarction severities, from partial to fully transmural scars, to understand their impact on tissue mechanics. To

Table 1
Comparison of the reported infarcted cardiac tissue elastic characterization protocols. AMFW stands for left ventricle anteromedial free wall, and AAFW for left ventricle anteroapical free wall.

Study	Subject	Sample location	Data collection time
Gupta et al. (1994) [21]	Sheep	AMFW	1–2–6 weeks
Holmes et al. (1997) [19]	Pig	AMFW	3 weeks
Zimmerman et al. (2000) [29]	Pig	AMFW	3 weeks
Fomovsky et al. (2010) [20]	Rat	AAFW	1–2–3–6 weeks
Zhang et al. (2010) [23]	Pig	AMFW-AAFW	2 days
Morita et al. (2011) [24]	Sheep	AAFW	8 weeks
Fomovsky et al. (2012) [18]	Rat	AMFW-AAFW	3 weeks
Mcgarvey et al. (2015) [22]	Pig	AMFW	1–4–8–12 weeks
Sirry et al. (2016) [26]	Rat	AMFW	0–1–2–4 weeks
Avazmohammadi et al. (2018) [5]	Sheep	AMFW	4 weeks
Mendiola et al. (2024) [28]	Rat	AAFW	0–1–2–3–4 weeks

the best of our knowledge, no previous study has performed such an extensive mechanical and microstructural evaluation across multiple infarction models and severities, including both extensive and compressive responses. We expect this more integrative approach will enhance our understanding of the global mechanical consequences of MI on cardiac tissue.

2. Materials and methods

2.1. Animals

A porcine animal model was selected due to its close resemblance to the human heart. Left ventricular transmural biopsy specimens were obtained from 12 white pigs (Sus scrofa domesticus) aged 18–22 weeks, with a mean weight of 72.46 ± 7.63 kg, divided into two groups. Another extra 13 animals were used as uninfarcted controls (C), which correspond to another recent study presented by the authors [6]. In 7 of the new animals, an antero-apical infarction was induced by occluding the Left Anterior Descending coronary artery (LAD). Two of these animals died before extraction, resulting in 5 animals in this group. Lastly, in the other 5 animals, an anteromedial infarction was induced by occluding the Left Circumflex coronary artery (LCX). All hearts were obtained from the Experimental Surgery Service of the Aragon Health Sciences Institute.

Healthy animals were directly euthanized under deep anesthesia using propofol (intravenous administration, up to 6 mg/kg) and inhaled sevoflurane (1.9%), followed by cardioplegic arrest. For additional details, refer to [6].

Infarcted animals were previously medicated. Namely, two weeks before the intervention, pigs received 400 mg/day of amiodarone (Sanofi) for 1 week and 200 mg/day for an additional week and 1 day before 300 mg aspirin (Bayer) and 300 mg clopidogrel (Sanofi). Pigs were then sedated with Tiletamina–Zolazepam (Virbac), and anesthesia was introduced with intravenous propofol (3 mg/kg, Teva), followed by 10–20 mg/kg/h continuous infusion and Remifentanil (18 μg/kg/h, Normon). Mechanical ventilation with a mixture of air and oxygen (1:1) at a tidal volume of 8–10 ml/kg was adjusted to maintain normocapnia and normoxia. BP and SpO2 were continuously monitored using the intensive cardiac monitor system (DASH 500 General Electric). After anticoagulation (heparin 10000 IU) and antiplatelet treatment (acetylsalicylic acid 450 mg), artery occlusion was performed. In 5 infarcted animals, LCX, the proximal left circumflex coronary artery was occluded by 90 min balloon inflation followed by reperfusion. In the other 5 infarcted animals, LAD, the left anterior descending coronary artery, was occluded equally. LCX infarctions were generated in the University of Navarra (Navarra, Spain), and LAD infarctions were generated in Jesús Usón Minimally Invasive Surgery Centre (Caceres, Spain). The animals were then transferred to Zaragoza for lairage until heart extraction. Infarctions were produced in two veterinary facilities for logistical reasons related to animal transport and scheduling. However, all surgical procedures were performed by the same cardiac surgery team following a unified protocol.

After extraction, all hearts were preserved in cold cardioplegia during transport to the laboratory, which took less than 2 h. All animal experiments adhered to the regulations of the local animal welfare committee for the care and use of experimental animals and were approved by local authorities (Ethics Committee on Animal Experimentation, CEAEA, of the Aragon region, reference code PI36/20).

In the LAD model, all animals (n = 5) exhibited a large transmural infarct extending to both the interventricular septum (IVS) and the Antero-Apical area of the left ventricle Free Wall, AAFW, affecting at least 30%–40% of the ventricular wall in all cases.

Conversely, the LCX model produced more heterogeneous infarctions among the five animals studied. In one of them (LCX-1), a small infarct (<1 cm^3) was observed in the most posterior part of the AMFW region. Two other animals (LCX-2 and LCX-5) had a series of localized infarctions close together in the AMFW, creating a sufficiently large area of partially infarcted tissue for biaxial testing (an infarcted area of at least 30 × 30 mm). The remaining two animals (LCX-3 and LCX-4) presented a transmural infarction in the AMFW area, similar to those in the LAD group. Although these infarctions also occupied the entire LV transmural thickness, the affected area was smaller than in the LAD model, impacting only about 10%–30% of the ventricular volume. Fig. 1 summarizes all the infarct types obtained in this study.

2.2. Biaxial testing

Specimens classification. As mentioned, the LCX and LAD infarctions affect the AMFW and AAFW zones of the LV, respectively. Consequently, we obtained samples for biaxial tests from both areas. Due to the heterogeneity observed in LCX model infarctions, where the proportion of infarcted tissue and its distribution along the thickness varied, we categorized the samples based on the infarction proportion and their location, rather than the animal of origin or the type of infarct. This resulted in eight distinct groups of samples. First, in the uninfarcted control animals, biaxial samples were taken from both the apical (i) and medial (ii) zones, A-C and M-C, respectively [6]. In both LCX and LAD animals, samples were also collected from areas remote from the infarct to analyze the influence of post-infarction remodeling in these regions. Thus, in LAD animals, besides the apical infarcted tissue, remote samples were collected from the medial zone (iii) and considered Non-Infarcted Tissue, M-NIT. Similarly, in LCX animals, samples were collected from the apical remote zone (iv), A-NIT.

In the case of LAD infarction, all animals exhibited transmural infarctions, so we only obtained samples of Fully Infarcted Tissue (v), A-FIT. For LCX infarcted animals, the infarctions were heterogeneous, leading to samples with varying distributions of infarcted tissue in the medial zone. These were divided into three groups: (vi) samples adjacent to the infarction but not containing any infarcted tissue, categorized as Transition Tissue, M-TT; (vii) samples containing both

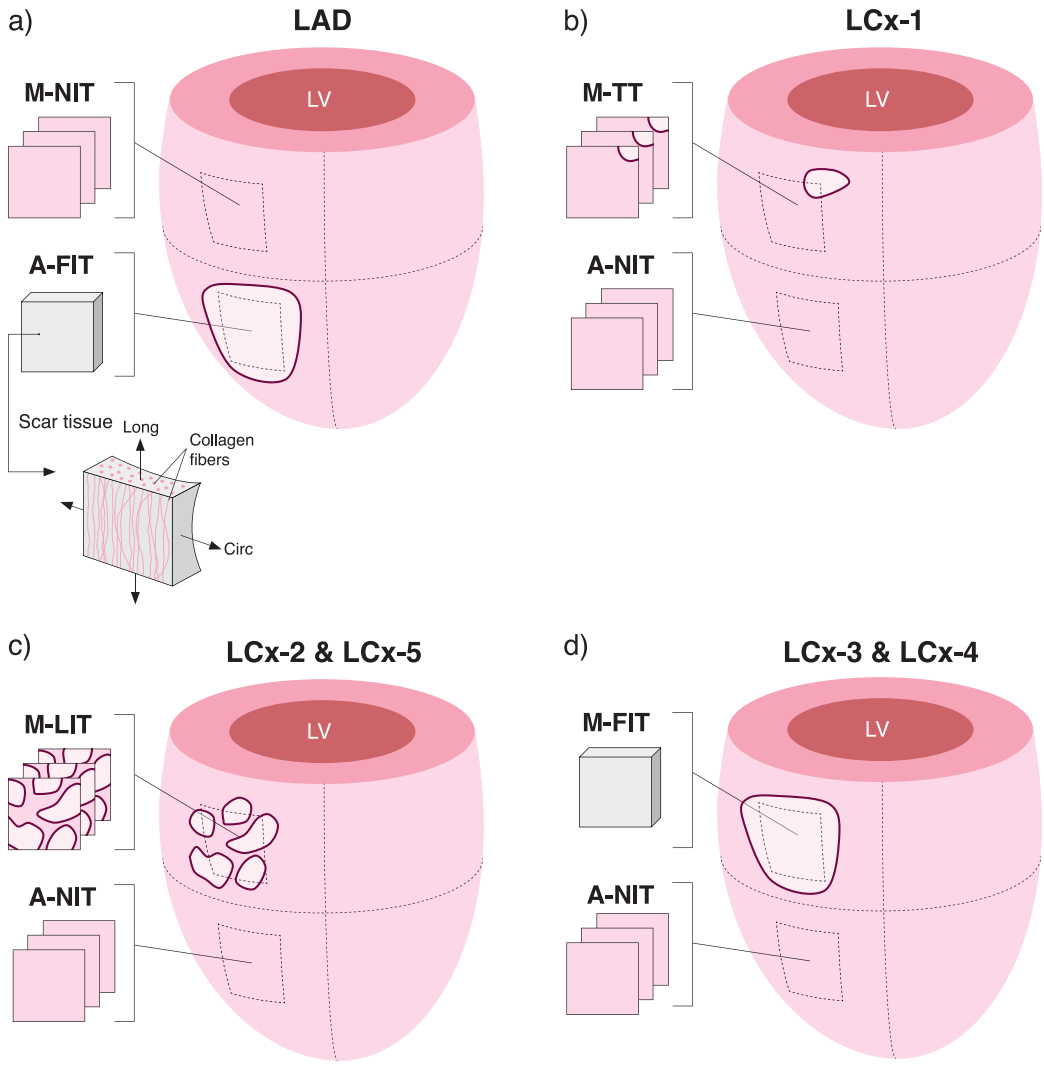

Fig. 1. Considered groups of infarcted hearts and biaxial samples. (a) LAD infarcted hearts: we obtained transmural apical fully infarcted samples (A-FIT), as well as remote thin slices at the medial region (M-NIT). (b) LCX single-infarction heart: thin non-infarcted proximal-to-infarction slices were obtained in the medial area (M-TT), and remote samples were also collected in the apical region (A-NIT). (c) LCX locally-infarcted hearts: thin slices of proximal non-infarcted (M-TT) or locally infarcted (M-LIT) tissue were obtained; remote samples were also collected at the apical region (A-NIT). (d) LCX fully infarcted hearts: transmural fully infarcted samples globally aligned (M-FIT) were cut similar to that of the LAD animals; remote samples were also collected at the apical region (A-NIT). FIT samples were globally oriented (along longitudinal–circumferential directions), while the rest of the samples were prepared MFD/CFD-aligned.

infarcted and healthy tissue, categorized as Locally Infarcted Tissue, M-LIT; and (viii) samples consisting solely of Fully Infarcted Tissue, similar to those from LAD animals, M-FIT.

In Table 2, a summary of all the biaxial tests classified by sample position is given, and in Table 3, we show a more in-depth classification for the infarcted tissue samples regarding the sample groups considered. Fig. 2 also shows some images of representative samples for all the considered groups. As shown in Figs. 2.b–c, not all the M-LIT samples present the same amount of infarcted tissue inside them. We consider as M-LIT all samples that presented any degree of infarcted tissue within them, even if it was a minor portion. We analyzed whether there were any differences between the M-LIT samples depending on their infarct content, and we did not see any significant variation (not shown).

Specimens preparation. For control, Non-Infarcted, Transition, and Locally-Infarcted samples, 35 × 35 mm transmural tissue blocks aligned with the global LV circumferential and longitudinal directions were cut using a single-edge razor blade, just as explained in [6]. Briefly, the tissue blocks were directly glued onto a vibratome cutting stage with the epicardium side down to ensure maximum longitudinal alignment of muscle fibers with the slicing plane [36–38], minimizing the number of transected fibers during sectioning [1,39,40]. Slices, 1 mm thick, were cut in freshly prepared ice-cold pre-oxygenated Tyrode's solution, advancing at a speed of 0.04 mm/s with an amplitude of 2 mm and a vibration frequency of 80 Hz. Calibration was performed before cutting each slice. Endocardial trabecular layers and areas of gross chordae tendineae from papillary muscles were trimmed, resulting in samples ranging from sub-endocardium to sub-epicardium. After slicing, sections were maintained in a cold cardioplegic solution and used for mechanical testing within the following 72 h. No mechanical differences were observed in the results within this timeframe. From these slices, 25 × 25 mm square specimens were prepared using a square cutter, with one side aligned with the mean-fiber direction (MFD) and the other with the cross-fiber direction (CFD), corresponding to the FF and NN directions in the LeGrice FSN coordinate system, respectively. Nine dot markers were applied to the specimens to later obtain the real sample stretches. Table 2 provides a summary of the tests performed.

For the fully infarcted tissue samples, A-FIT and M-FIT, the vibratome could not slice the tissue due to significant changes in structure and stiffness. Therefore, a single transmural sample was obtained, ranging from subendocardium to subepicardium. The thickness of these

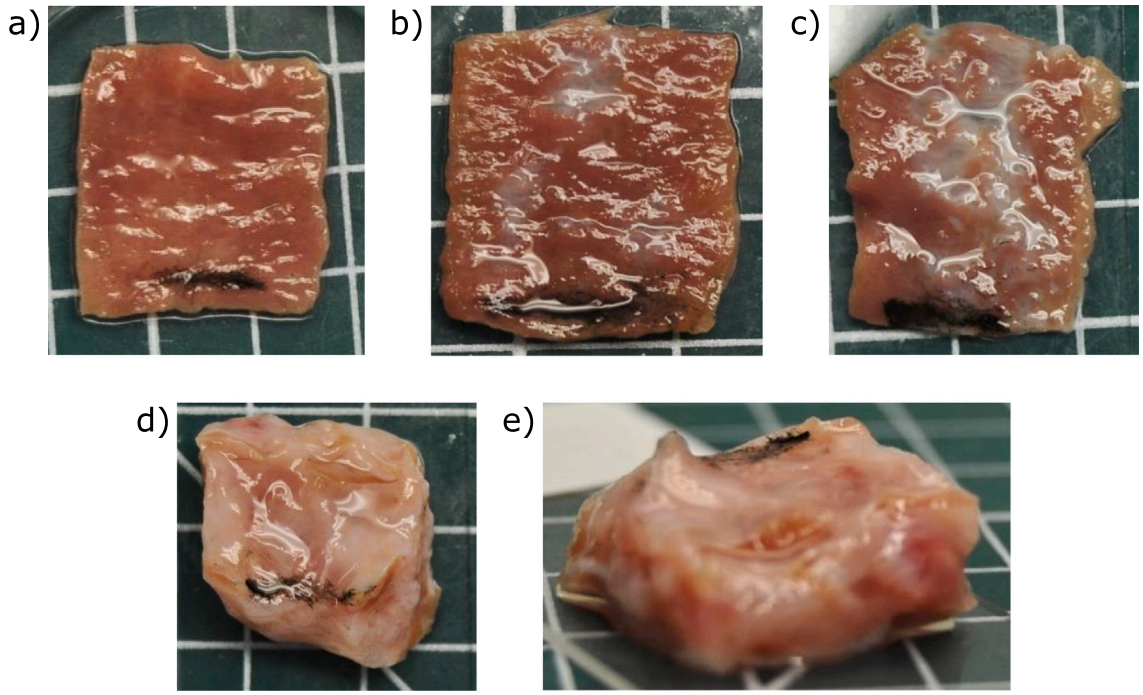

Fig. 2. Infarcted tissue samples examples. (a) LCX medial transitional tissue sample, M-TT, with no infarcted tissue contained. (b–c) LCX medial locally infarcted tissue samples, M-LIT. We show two examples, one in which the infarcted area (in whitish tones) is (b) relatively small and the other where (c) is bigger. (d–e) LCX medial fully infarcted tissue sample, M-FIT. Black lines indicate MFD in all samples except for FIT tissue, where they indicate the LV global circumferential direction.

transmural samples can be consulted in Table 4. In both infarction models, the amount of fully infarcted tissue available for obtaining biaxial samples was very limited, allowing for only one square sample per animal, approximately 20–25 mm on each side. Since orienting the slices according to local main and cross-fiber directions was not possible, the samples were aligned with the global circumferential and longitudinal directions of the LV. Hence, special caution should be paid when comparing these results with those from other samples. The sample preparation protocol was the same as the other.

Biaxial Extension Protocol. Biaxial tests (Bx) were conducted using biaxial testing equipment (Instron Planar Biaxial Soft Tissue Test System) with a 10 N load cell, following the protocol established by [3]. Four different stretch levels (5%–20% in 5% increments) were applied consecutively, each with 4 preconditioning cycles and 1 measuring cycle to ensure a stable response, which has been proven to be sufficient preconditioning for myocardium [3]. Various loading ratios between MFD and CFD were applied at each stretch level (1(MFD):1 (CFD), 1:0.75, 1:0.5, 0.75:1, 0.5:1) to capture the direction-dependent material response. All tests were performed with a 2 mN equibiaxial preload under quasi-static conditions (v = 2 mm/min). Samples were kept in cardioplegia solution at 37 °C to prevent cellular contraction. The mechanical response was evaluated using the Cauchy stress vs stretch as indicated in [6]. To monitor the real sample deformations, nine dots were marked at the center of the biaxial sample using a waterproof marker. Shear strains and stresses were computed as described in [41].

We also evaluated the variation of cross-coupling effects across the different sample groups. In-plane coupling occurs when the stress measured in a given testing direction depends on the loading ratio applied in the transversal direction. Conversely, in the absence of cross-coupling, the mechanical response in each direction would remain independent of the transversal load. To quantify this effect, we computed the Cross-Coupling Ratio (CCR) for each testing direction. CCR was defined as the relative reduction in peak stress at a non-equibiaxial loading ratio with respect to the peak stress obtained under the 1:1 equibiaxial condition. For instance, for the MFD direction at a 1:0.75 loading ratio, CCR is given by

$$CCR = 1 - \frac{\sigma_{1:0.75}^{\max}}{\sigma_{1:1}^{\max}}. \quad (1)$$

2.3. Simple triaxial shear testing

Specimen preparations. To ensure uniform fiber orientation within each specimen, we used cubic samples as small as feasible. We manually cut 4 mm cubic samples aligned to the local LeGrice FSN axes [1] using a vibratome blade, and Evans blue dye for easier structural identification. Specimens were harvested from the Posterior-Medial area of the LV Free Wall (PMFW) in all groups, chosen as a non-infarcted region in infarcted animals (Fig. 3.b).

Triaxial Shear Protocol. Simple triaxial shear tests (STS) were performed using a CellScale MicroTester G2, following the protocol outlined by [2]. Briefly, five incremental stretch levels (10%–50% in 10% steps) were applied sequentially, with two preconditioning cycles and one measurement cycle at each level. Both for Bx and STS tests, we corroborated that the myocardial tissue can reach a steady state after the selected preconditioning cycles. Each sample was tested in only one shear mode. At least one test was performed in each of the six shear modes for each animal (Table 2). All shear tests were also conducted under quasi-static conditions (v = 2 mm/min) and maintained in cardioplegia solution at body temperature (37 °C) to prevent cellular contraction. All tests were completed within 72 h of heart extraction. The shear engineering strain (γ) and shear stresses (τ) were evaluated (see [6]).

2.4. Confined compression testing

Specimen Preparation. As shown in Fig. 3.c, compression samples were processed from the AMFW region, distant from the infarcted tissue. Due to spatial constraints, obtaining compression samples directly from the infarcted tissue was generally not feasible, except in specimen (LCX-4), where we managed to assess the compressibility of a few

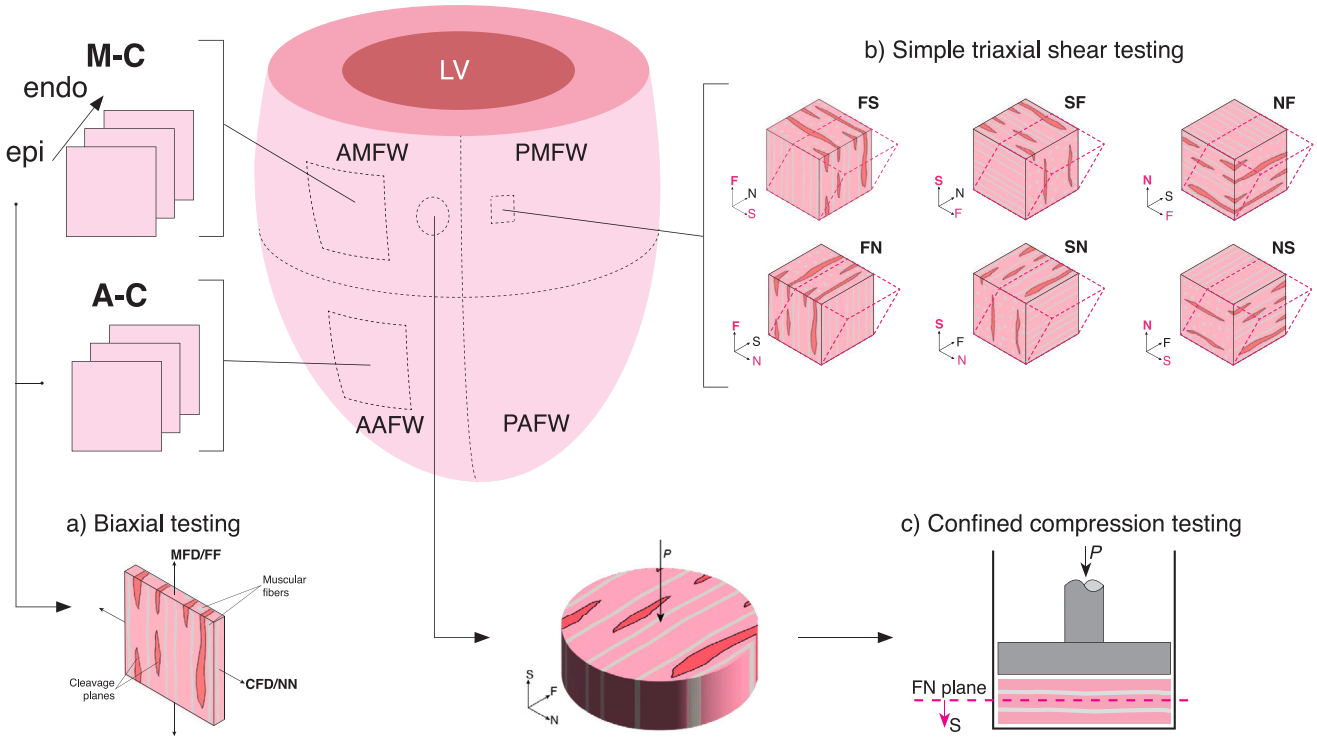

Fig. 3. Considered mechanical tests summary. All tests followed the same protocols and conditions as explained for healthy tissue characterization. Testing groups' classification by tissue condition will be detailed below. (a) Biaxial testing; (b) Triaxial shear testing; (c) Confined compression testing.

infarcted samples (n = 4). Similar to the biaxial tests, samples were extracted from the initial 35 × 35 mm slices, but this time, slices were cut with a thickness of approximately 2 mm. Then, cylindrical samples with a diameter of 6 mm were prepared, ensuring that the circular section aligned with the FN plane. Consequently, the compression load was applied along the S direction (Fig. 3.c).

Confined compression protocol. Confined compression tests (CC) were conducted following the protocol outlined by [9]. A total of 82 CC tests were performed (Table 2). Specimens were placed in a rigid chamber matching their transverse dimensions. Compression was applied using a uniaxial machine (Instron MicroTester I5848 with a 500 N load cell) under quasi-static conditions (v = 2 mm/min). The specimens were compressed until reaching a volumetric strain of 10%. Due to the confined nature of the test, the axial strain equaled the volumetric strain. All tests were completed within 72 h post-heart extraction. Volumetric strain (J) and hydrostatic stress (P) were calculated as indicated in [6].

2.5. Histological analysis

Histological analysis was the same as in [6]. Briefly, sample processing was carried out at the Central Anatomical Pathology Unit of the Aragon Health Sciences Institute. Formaldehyde-fixed samples were processed in cassettes using an automated tissue processor (Tissue-Tek Xpress x50). Tissue blocks were created using a Leica EG1150 unit and solidified on a cold plate. Paraffin-embedded samples were sectioned into 3 μm thick slices with a Leica RM2255 rotary microtome and kept in a tempered bath. The sections were then collected onto Superfrost Plus slides (Bio-optica Labolan Ref. [50559]). Slides were placed on vertical racks to dry overnight at 37 °C, followed by a deparaffinization and hydration process. The sections were subsequently stained using Picrosirius Red (PR) under polarized light, Masson's Trichrome (M3), and Hematoxylin–Eosin (HE) to visualize the distribution of muscular and collagenous fibers. After staining, the sections were dehydrated by immersing them in ascending alcohol solutions (70%, 96%, and 100%) for 15 s each. Lastly, all sections were cleared with xylene for 15 s and mounted on the Leica CV5030 automatic mounter using Epredia glass coverslips.

2.6. Quantitative histological analysis of collagen organization

Collagen content was quantified in Sirius Red-stained histological sections (n = 18 per animal) at 10× magnification. Bright-field images were analyzed in MATLAB using color thresholding to isolate the red-stained collagen areas. Collagen percentage was calculated as the ratio of collagen-positive pixels to the total tissue area, excluding background regions. Subsequently, the same Sirius Red-stained sections were examined under polarized light microscopy to differentiate collagen types I and III based on their birefringence properties. Collagen type I was identified by its strong orange–red tone, whereas type III appeared greenish. The relative proportion of each collagen type was then quantified using the same image analysis procedure.

Collagen fiber orientation in myocardial tissue was assessed using the OrientationJ plugin in ImageJ [42]. Polarized light microscopy images were analyzed to obtain orientation distribution histograms and color-coded vector maps, from which the dominant fiber direction and angular dispersion were computed relative to the circumferential axis. Orientation histograms from all analyzed fields were then averaged to generate a single representative distribution per scar.

2.7. Statistical analysis

The Shapiro–Wilk test was applied to assess the normality of each subgroup's results. Then, p-values were calculated using Student's t-test for normally distributed samples and the Mann–Whitney U test for non-normally distributed samples, with $p < 0.05$ considered significant. Statistical analyses were conducted using a custom MATLAB R2024a program. All data values are reported as mean ± standard deviation (SD).

Table 2
Mechanical tests by sample location and test type. AMFW: Antero-Medial Free Wall; AAFW: Antero-Apical Free Wall; PMFW: Postero-Medial Free Wall.

Animal	Biaxial (AMFW)	Biaxial (AAFW)	Shear (PMFW)	Compression (AMFW)
C-1	3	–	6	–
C-2	3	–	6	–
C-3	2	–	7	–
C-4	2	–	6	–
C-5	2	–	7	–
C-6	2	–	6	–
C-7	2	–	7	–
C-8	1	4	–	3
C-9	2	4	–	8
C-10	1	5	–	2
C-11	1	4	–	–
C-12	–	5	–	–
C-13	3	2	–	7
Total C	**24**	**24**	**45**	**20**
LCX-1	6	1	6	5
LCX-2	5	–	6	4
LCX-3	5	–	11	15
LCX-4	4	1	8	14
LCX-5	3	1	6	6
Total LCX	**23**	**3**	**37**	**44**
LAD-1	2	1	6	3
LAD-2	2	1	6	3
LAD-3	3	1	6	3
LAD-4	2	1	8	3
LAD-5	3	1	13	6
Total LAD	**12**	**5**	**39**	**18**

Table 3
Classification of the infarcted tissue biaxial tests by tissue conditions. A-NIT: LCx apical non-infarcted tissue; M-NIT: LAD medial non-infarcted tissue; M-TT: LCx medial adjacent transition tissue; M-LIT: LCx medial locally infarcted tissue; M-FIT: LCx medial fully infarcted tissue; A-FIT: LAD apical fully infarcted tissue.

Animal	A-NIT	M-NIT	M-TT	M-LIT	M-FIT	A-FIT
LCX-1	1	–	5	1	–	–
LCX-2	–	–	–	5	–	–
LCX-3	–	–	4	–	1	–
LCX-4	1	–	–	3	1	–
LCX-5	1	–	–	3	–	–
Total LCX	**3**	**–**	**9**	**12**	**2**	–
LAD-1	–	2	–	–	–	1
LAD-2	–	2	–	–	–	1
LAD-3	–	3	–	–	–	1
LAD-4	–	2	–	–	–	1
LAD-5	–	3	–	–	–	1
Total LAD	**–**	**12**	**–**	**–**	**–**	**5**

3. Results

3.1. Infarcted tissue morphology

Apart from the differences in the mechanical properties of the tissue, the geometric characteristics and the subsequent remodeling process varied significantly for each type of infarction. First, as mentioned above, the LCX model generated highly heterogeneous infarctions. In the LCX-1 animal, a single small focal infarction (<1 cm^3) was observed, which was not even transmural. This was located in the most posterior-basal area of the AMFW region, with no indications of any other infarcted tissue in the entire ventricular wall. Despite the heart being collected six weeks post-infarction, we did not observe any transmural remodeling, maintaining a wall thickness similar to control hearts (around 10–15 mm).

Secondly, the LCX-2 and LCX-5 hearts presented several local infarctions close to each other, creating an infarcted area that occupied most of the AMFW region (approximately a 25–30 mm-sided square cross-sectional area). In this case, infarctions were observed throughout the entire ventricular thickness, although not homogeneously. However, no transmural thinning was observed in these cases either, suggesting that, when a significant transmural infarction is not achieved, the geometry of the ventricle remains fairly stable compared to the physiological state, at least up to six weeks after the cardiac event.

Lastly, LCX-3 and LCX-4 hearts presented a complete transmural infarction, occupying a 20–25 mm sided area of the AMFW region. We observed a significant macroscopic geometrical remodeling, with a thickness reduction of about 45%–60% in the infarcted area. The rest of the ventricle maintained a similar thickness to that of the control hearts. Physiological thickness was recovered in less than 1 cm from the infarcted area. Table 4 summarizes some of the most representative infarction dimensions for each heart. We have considered the minimum thickness reached at the infarcted area (IT-Th); the length of the LV free wall infarcted area (IT-L), assuming a rounded-like shape; and the wall thickness far from the infarction (HT-Th).

Regarding the LAD animals, all exhibited a complete transmural infarction, similar in many aspects to LCX-3 and LCX-4. In this case, the infarctions were also completely transmural, with significant wall thickness reductions in the infarcted area as well (Table 4). The LAD infarctions had a greater extent than the LCX ones since, in addition to the infarcted part of the AAFW (about 20–30 mm side), a large area of infarcted tissue was also observed in the IVS, occupying much of its apical part. We focused on the characterization of the LV free wall, so IVS was not considered. A summary of the remodeled geometries is given in Fig. 4.

3.2. Histological analysis

3.2.1. Hematoxylin–Eosin staining

Here we show representative histological results under HE, M3, and PR staining. Again, all samples correspond to planes parallel to the epicardium, and all conclusions regarding fiber orientation refer to the local orientations within these slices. First, HE staining for all groups of samples is shown in Fig. 5. HE exclusively enables the analysis of muscle fiber distribution, coloring them in reddish or pinkish tones. Therefore, HE results will be used to analyze the organization and directionality of the muscle fibers in each case. We present results from the control groups, both medial (M-C, Fig. 5.a) and apical (A-C, Fig. 5.j); tissue remote to the LCX (A-NIT, Fig. 5.k) and the LAD infarctions (M-NIT, Fig. 5.b); the LCX transition tissue (M-TT, Fig. 5.c); the LCX locally infarcted tissue (M-LIT, Figs. 5.d,e,g,h,i); the LCX fully infarcted tissue (M-FIT, Fig. 5.f); and the LAD completely infarcted tissue (A-FIT, Fig. 5.l).

The control images, M-C and A-C (Figs. 5.a and j, respectively), correspond to AMFW and AAFW regions of the 4MA animals described in [6], respectively. Very briefly, in M-C, the fibers show a strong alignment around MFD, with a very ordered structure. On the other hand, in A-C, there is still a certain alignment around MFD but lower, presenting a greater fiber dispersion that becomes almost random in some regions.

Continuing with the tissue remote to the infarction (Figs. 5.b,k), both A-NIT and M-NIT samples presented a very similar structure to the physiological state, almost identical to that of the control samples. Thus, neither LAD nor LCX infarctions seem to influence cardiomyocyte orientation in remote areas.

Fig. 5.c shows the structure of M-TT samples, which correspond to adjacent tissue to the LCX infarcted region but do not contain infarcted tissue itself, to assess the MI's immediate repercussions on its vicinity. HE staining also revealed a structure identical to the physiological state, with no variations in muscle alignment compared to M-C or M-NIT samples. Although this will be revisited with the other contrasted stainings, there appears to be no evident effect on muscle alignment in

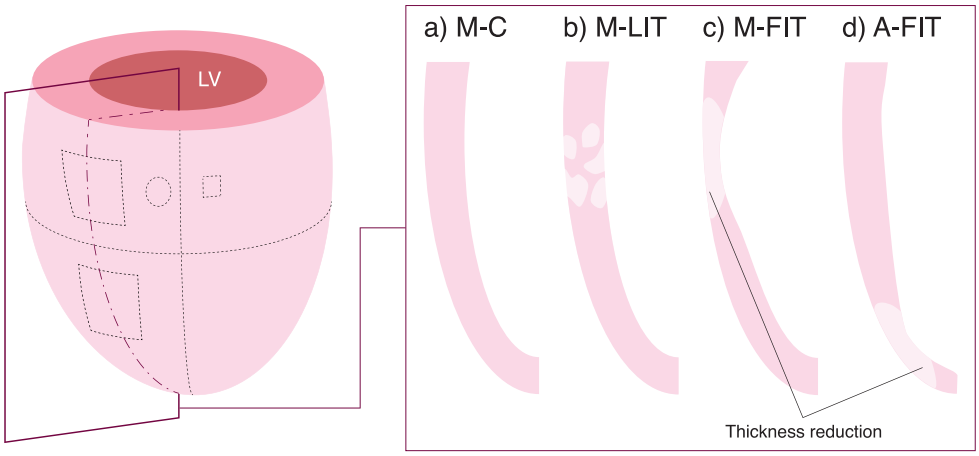

Fig. 4. Infarcted hearts thinning summary. (a) Control non-infarcted hearts, no wall thickness reduction observed. (b) Locally infarcted hearts, no wall thickness reduction observed. (c) Medial and (d) apical transmurally infarcted hearts, significant thickness reduction was observed in the infarcted area.

Table 4
Infarcted tissue representative dimensions. IT-Th: Infarcted area minimum thickness; IT-L: Infarcted area estimated length; HT-Th: Healthy tissue control thickness.

Sample	LAD-1	LAD-2	LAD-3	LAD-4	LAD-5	Mean ± SD
IT-Th (mm)	4.8	4.1	5.1	6.2	5.4	5.1 ± 0.7
IT-L (mm)	29	26	24	21	27	25.4 ± 3.1
HT-Th (mm)	12	13	10	15	10	12.0 ± 2.0
Sample	LCx-1	LCx-2	LCx-3	LCx-4	LCx-5	Mean ± SD
IT-Th (mm)	–	–	5.0	6.1	–	5.55 ± 0.6
IT-L (mm)	8	27	21	26	23	21.0 ± 8.2
HT-Th (mm)	12	14	13	12	11	12.4 ± 1.1

the M-TT tissue, suggesting a highly localized effect of both LAD and LCX infarctions, confined to the scarred area.

In Figs. 5.d,e,g,h,i, several sections of locally infarcted tissue (M-LIT) are presented. All these samples originate from the AMFW zone; therefore, a defined cardiomyocyte orientation around the MFD direction is expected in all of them. Non-infarcted tissue appears with a more intense pinkish tone, whereas infarcted areas show a whitish tone. Within the infarcted regions, blue–violet cell nuclei are still identifiable, suggesting that the scar comprises not only newly deposited components such as collagen but also necrotic myocytes. The structure of the scar will be revisited when discussing the M3 and PR stains and examined in greater detail in the collagen quantification section. First, at interfaces where healthy tissue abuts infarcted tissue, multiple patterns were observed. In some of them, muscle fibers maintained a preferential local orientation similar to the physiological state (Fig. 5.d). In others, this orientation was fully or partially disrupted (Figs. 5.e,h), presenting patterns more akin to those of the AAFW zone. We also identified extensive regions of infarcted tissue (Fig. 5.i) and of preserved healthy tissue (Fig. 5.g). All these findings indicate substantial heterogeneity within partial infarcts, which will probably result in mechanical properties distinct from those of physiological myocardium

Lastly, fully infarcted tissue exhibited a high collagen content, with almost no visible muscle (Figs. 5.f,l), as reflected by the whitish appearance. Accordingly, scar tissue will be analyzed in the following sections.

3.2.2. *Masson's Trichrome staining*

Secondly, M3 staining results are shown in Fig. 6. M3 highlights muscle tissue in reddish–purplish tones and collagen I in bluish tones. Thus, we use M3 staining to describe collagen distribution. Specifically, collagen distribution is analyzed qualitatively here, as it will be examined in greater detail in Section 3.2.4. Again, we present results for all contrasted groups (M-C, A-C, M-NIT, A-NIT, M-TT, M-LIT, M-FIT, and A-FIT).

Again, remote areas (Figs. 6.b,k) exhibit an almost identical response to physiological tissue (Figs. 6.a,j). All four images show a very weak collagen network, nearly imperceptible under M3. This trend is also consistent in the near-infarction area, M-TT, where no evident microstructural changes are observed either (Fig. 6.c).

The M-LIT samples show different collagen distributions, similar to those seen with HE staining. This tissue exhibits both large bundles of collagen fibers aligned with the physiological preferential direction of the muscle fibers (Fig. 6.d), and more dispersed collagen structures lacking clear directionality (Fig. 6.e). In both patterns, collagen is now clearly visible within the infarcted tissue, becoming its predominant component. The collagen fibers form a more reticulated and wavy network, contrasting with the straighter muscle fibers (Fig. 6.d). Additionally, changes were observed in the collagen composition of the non-infarcted regions within M-LIT samples, with a notable increase in perimysial collagen along cleavage planes (Fig. 6.g), indicating that partially infarcted tissue undergoes microstructural remodeling not only in scarred but also in adjacent, apparently unaffected, areas. This suggests that, in the infarct vicinity, in addition to the replacement of healthy tissue by collagen, interstitial fibrosis may also occur, although it was only observed immediately adjacent to infarcted zones. This interstitial fibrosis resembles what we previously reported in our study on remodeling associated with aging and hypertrophy in older animals, which led to marked changes in the mechanical response of the tissue [6].

In the fully infarcted samples from the medial zone (M-FIT), an intense collagen structure with clear directionality was observed (Fig. 6.f). Here, collagen forms long fibers strongly oriented within the sample plane (parallel to the epicardium), as the observed chains are not sectioned. The wavy nature of the collagen fibers is prominent, with no other muscular components visible across large sections. In some localized regions, slightly more irregular collagen patterns appear (Fig.

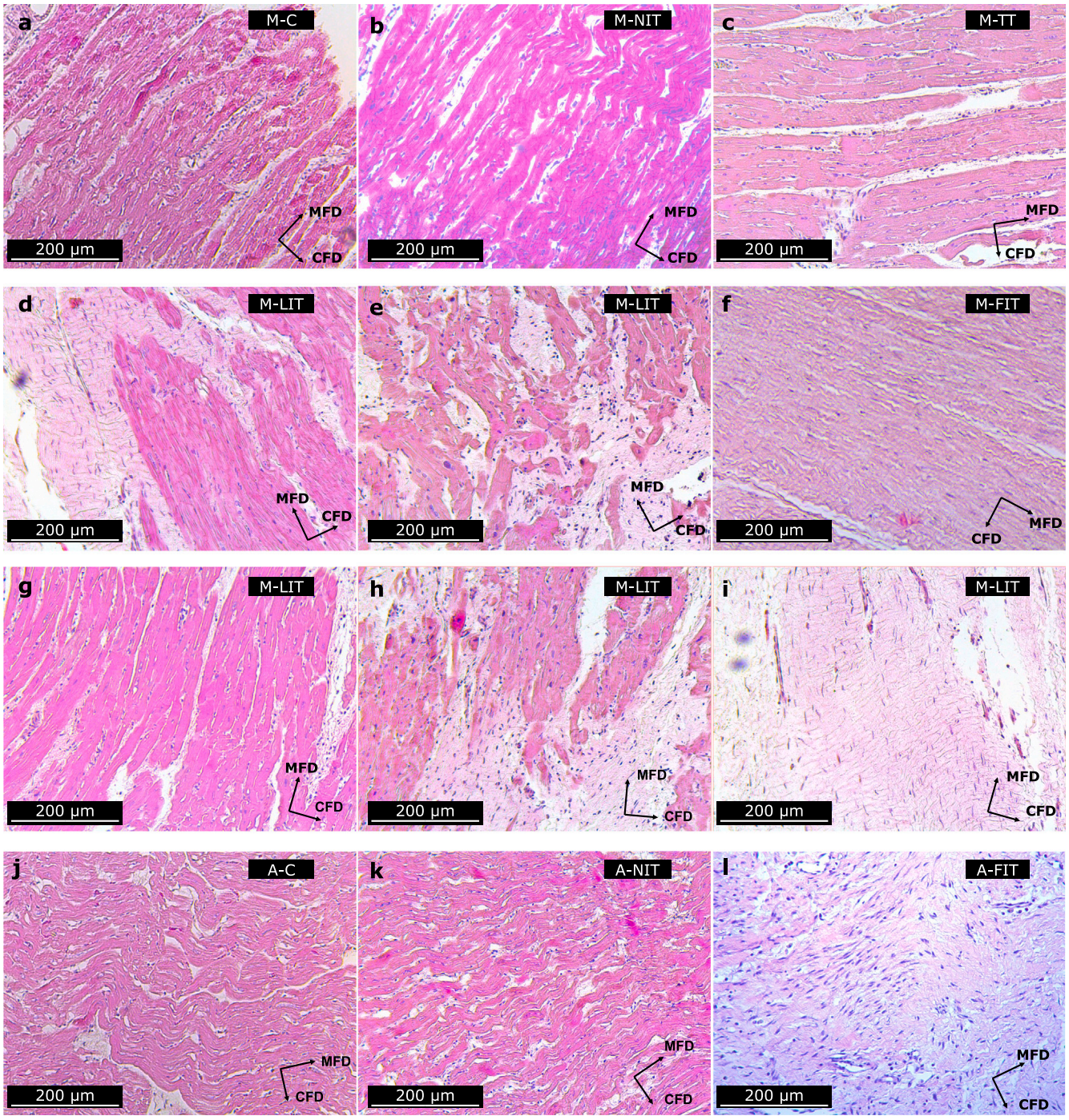

Fig. 5. Results of the histological analysis under Hematoxylin–Eosin (HE) staining. Contrasted samples at the AMFW region: (a) control samples, M-C; (b) remote non-infarcted tissue (LAD hearts), M-NIT; (c) transitional tissue (LCx hearts), M-TT; (d–e–g–h–i) locally infarcted tissue (LCx hearts), M-LIT; (f) fully infarcted tissue (LCx hearts), M-FIT. Contrasted samples at the AAFW region: (j) control samples, A-C; (k) remote non-infarcted tissue (LCx hearts), A-NIT; (l) fully infarcted tissue (LAD hearts), A-FIT. Global Main and Cross Fiber Directions are indicated as MFD and CFD for each image.

6.h), although a preferential orientation is still identifiable. Overall, this preferential collagen alignment follows the original direction of the muscle fibers, which in the AMFW is predominantly circumferential (Fig. 6.i), suggesting that the collagen network develops along the native orthotropic directions of the healthy myocardium. This will be analyzed in greater detail in Section 3.2.4.

In the apical zone, A-FIT, extensive collagen networks were also observed (Fig. 6.l). However, in this region, the collagen fibers exhibited a much more random and chaotic orientation. Here, the wavy pattern of the collagen fibers is even more evident. This is well related to the physiological structure of the tissue in this area, which is naturally more dispersed.

3.2.3. *Picrosirius Red staining*

Lastly, PR staining results are shown in Fig. 7. PR staining facilitates collagen fiber visualization, with collagen-I appearing in yellowish and reddish tones under polarized light, and collagen-III in greenish tones. Thus, we will use the PR results as well to gain more insights into the collagen distribution for all the above groups.

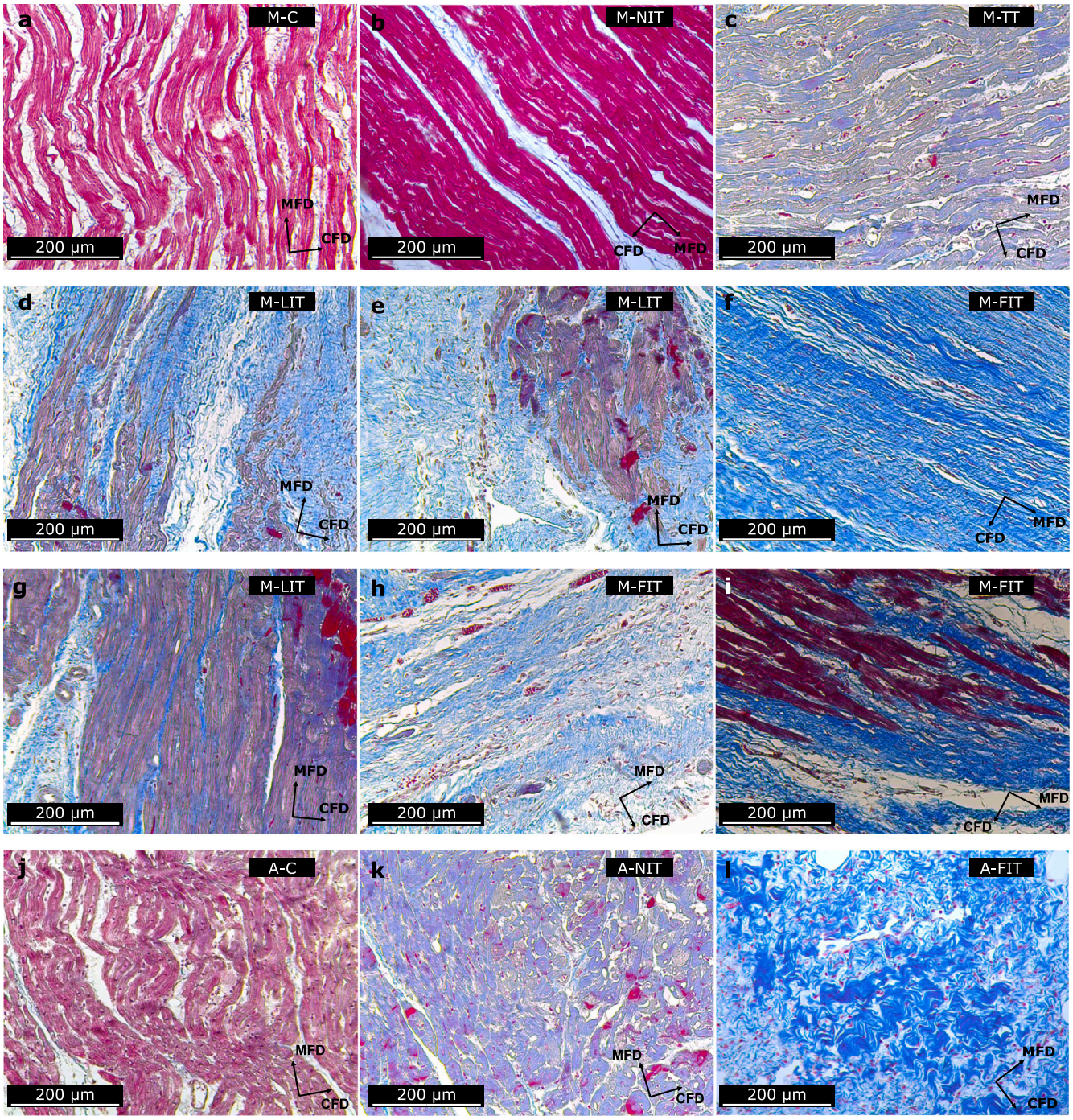

Fig. 6. Results of the histological analysis under Masson's Trichrome (M3) staining. Contrasted samples at the AMFW region: (a) control samples, M-C; (b) remote non-infarcted tissue (LAD hearts), M-NIT; (c) transitional tissue (LCx hearts), M-TT; (d–e–g) locally infarcted tissue (LCx hearts), M-LIT; (f–h–i) fully infarcted tissue (LCx hearts), M-FIT. Contrasted samples at the AAFW region: (j) control samples, A-C; (k) remote non-infarcted tissue (LCx hearts), A-NIT; (l) fully infarcted tissue (LAD hearts), A-FIT. Global Main and Cross Fiber Directions are indicated as MFD and CFD for each image.

The results for the M-C, A-C, M-NIT, and A-NIT groups are consistent with the M3 staining, so they will not be discussed again (Figs. 7.a,b,j,k). Similarly, the M-TT tissue shows a response very similar to the physiological one, with collagen present only in the cleavage planes (Fig. 7.c). In all these cases, only collagen-I is identified, as indicated by the reddish tones.

The partially infarcted tissue, M-LIT, exhibits areas with structured collagen (Fig. 7.d) and others with a random distribution (Fig. 7.e). As will be further explored in next section, in Fig. 7.i fibers with visible yellowish shades are slightly observed, which may suggest the presence of collagen-III [43]. Furthermore, besides the fibers following the MFD direction, a wavy pattern is seen in the transverse direction, indicating that the collagen network is not only structured around the muscle fibers but also extends transversely, forming an intricate in-plane structure. The unaffected areas also show a collagen increase within the cleavage planes (Figs. 7.g,h).

For the fully infarcted samples, both A-FIT and M-FIT, the results are very similar to those obtained with M3 staining. The medial tissue again shows a highly directional distribution, with an intense collagen network (Fig. 7.f). In the apical zone (Fig. 7.l), a very dense collagen

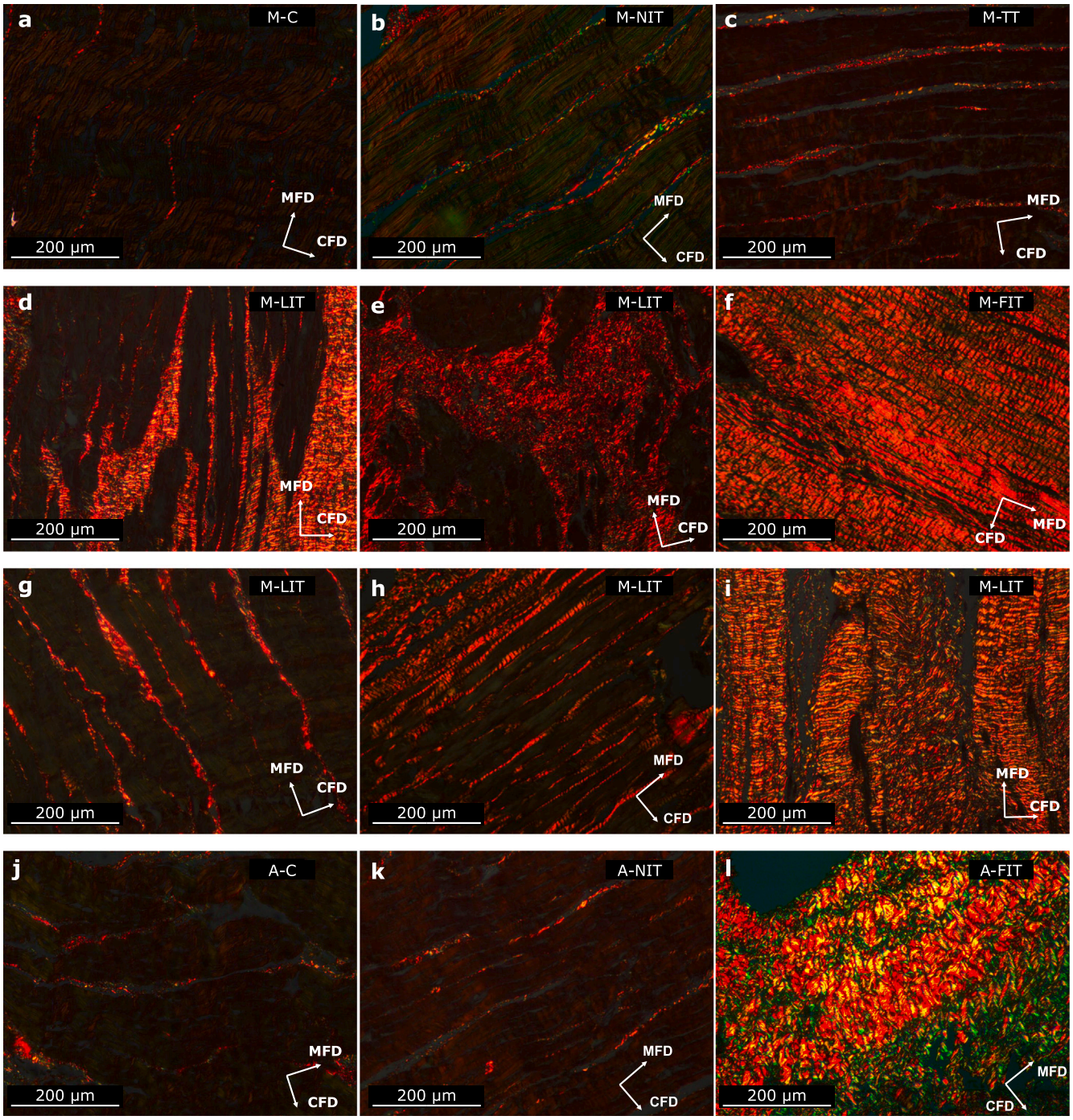

Fig. 7. Results of the histological analysis under Picrosirius Red (PR) staining. Contrasted samples at the AMFW region: (a) control samples, M-C; (b) remote non-infarcted tissue (LAD hearts), M-NIT; (c) transitional tissue (LCx hearts), M-TT; (d–e–g–h–i) locally infarcted tissue (LCx hearts), M-LIT; (f) fully infarcted tissue (LCx hearts), M-FIT. Contrasted samples at the AAFW region: (j) control samples, A-C; (k) remote non-infarcted tissue (LCx hearts), A-NIT; (l) fully infarcted tissue (LAD hearts), A-FIT. Global Main and Cross Fiber Directions are indicated as MFD and CFD for each image.

network is also observed. Here, collagen-III is especially evident. However, as presented in the following section, collagen-III was detected in both M-FIT and A-FIT. In A-FIT, collagen fibers do not form long, highly reticulated structures, and fiber alignment in this area remains low.

3.2.4. Quantitative histological analysis of collagen organization

Fig. 8 summarizes the structural collagen analysis for the infarcted samples. First, the total collagen content of each infarcted tissue group is shown (Fig. 8.a). A clear increase in collagen is observed with the degree of infarction, as expected, with M-FIT and A-FIT samples showing the highest percentages. Among them, the apical samples (A-FIT) exhibit the greatest collagen density per area, with this difference being statistically significant ($p < 0.01$). Next are the partially infarcted samples (M-LIT), which, although not reaching the levels of the fully infarcted groups ($p < 0.05$ vs. both M-FIT and A-FIT), still present significantly higher collagen content than M-TT samples ($p < 0.01$). In this case, variability is the highest among all groups, consistent with the previously discussed heterogeneity in structure and organization for

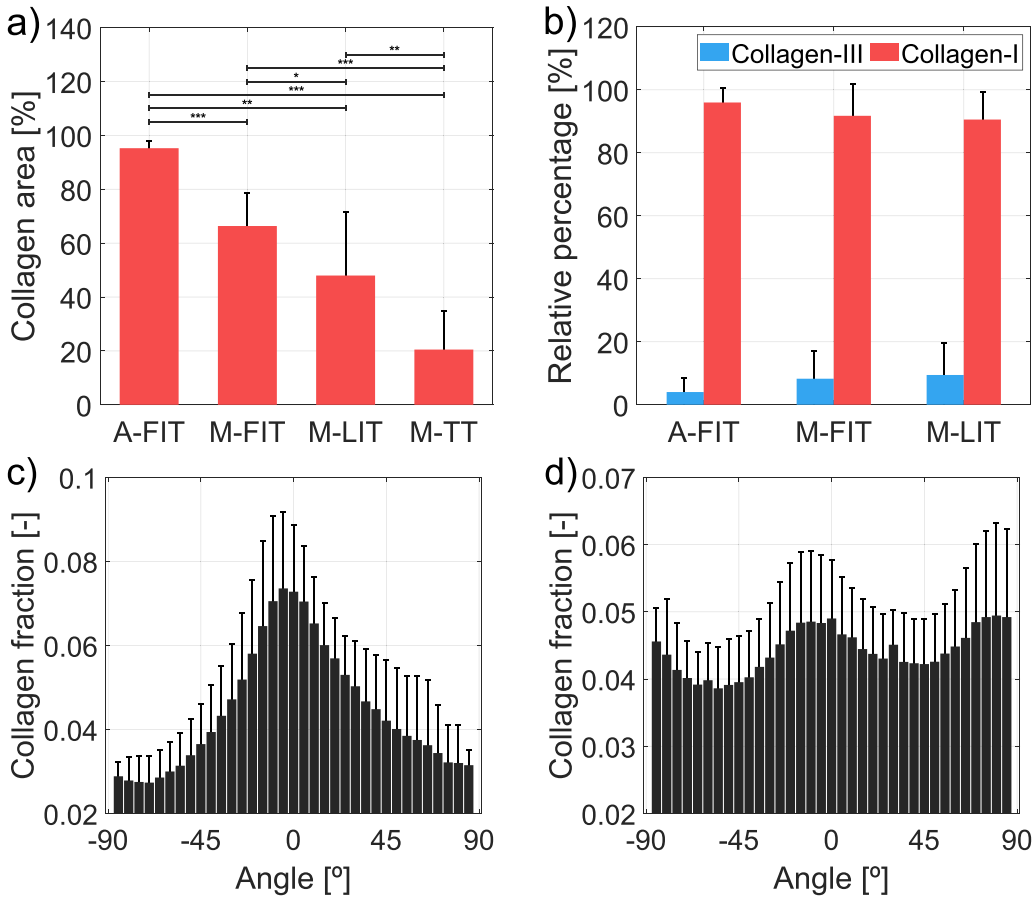

Fig. 8. Collagen quantification results. (a) Total collagen content in infarcted tissue groups (A-FIT, M-FIT, M-LIT, and M-TT). (b) Relative quantification of collagen-I and collagen-III in partially and fully infarcted samples (M-LIT, M-FIT, and A-FIT). Mean histograms of collagen fiber orientation for M-FIT samples (c), and for A-FIT samples (d). In (a), statistical significance is indicated as $p < 0.05$ (*), $p < 0.01$ (**), and $p < 0.001$ (***).

these samples. Finally, the M-TT samples show the lowest collagen content, with relatively high dispersion as well. These values are very close to those of physiological or remote tissue (not shown), as described in the previous sections.

Following the total collagen quantification, Fig. 8.b shows the analysis of the relative amounts of collagen-I and collagen-III for each sample type. In this case, M-TT samples are not included, since only collagen-I was consistently observed as described in Section 3.2.3. Across all groups, collagen-I is the predominant component (>90% in all cases), consistent with the visual assessment discussed earlier. No statistically significant differences were found between groups for either collagen-I or collagen-III. Although visually A-FIT samples appeared to have more collagen-III, the structural analysis confirmed that this difference was not statistically significant ($p > 0.05$). Therefore, all groups are characterized by a predominance of collagen-I and less than 10% collagen-III, with no significant differences between them.

Finally, Figs. 8.c–d compare the spatial distribution of collagen fibers within the cutting planes (parallel to the epicardium) for the fully infarcted medial and apical samples (M-FIT and A-FIT, respectively). This comparison is particularly relevant because these two groups showed the highest overall collagen content but differed markedly in organization. In medial infarcts, collagen fibers are preferentially aligned around the global circumferential direction (0°), whereas in apical infarcts, no clear orientation is observed, resulting in a nearly isotropic distribution. These findings are consistent with previous reports [18,20].

3.3. Mechanical response of healthy myocardium

In Fig. 9.a, we present a summary of the averaged biaxial results for all the loading ratios at 20% stretch for the control animals, both for M-C and A-C. All plots show Cauchy stress vs. stretch results. We focus solely on the elastic part of the response, neglecting the viscoelastic behavior. Myocardial tissue exhibits a highly non-linear and anisotropic response, with higher stiffness in the MFD (FF) direction than in the CFD (NN) one, as expected. A-C results ($n = 24$) show a slightly less stiff and more isotropic response than M-C ($n = 24$), with a significant reduction ($p < 0.02$) in peak stress values of 24.6% and 14.2% in each MFD and CFD, respectively. As shown in the histological analysis, these minor variations may be related to differences in the architecture of muscle fibers in these two regions.

Fig. 9.e shows the averaged results from the STS characterization for all 6 configurations (at least $n > 8$ in each shear mode). Again, STS exhibits a highly non-linear response, with an evident orthotropic behavior, which can be differentiated into three groups. First, tests, where the shear stress is mainly absorbed by the F direction (FN-FS), show the stiffest response, then those where the shear stress is mainly in the S direction, and last, those in which the shear stress falls mainly on the N direction (NF-NS). This is consistent with several results in the literature [2–5].

Lastly, control animals' CC results are shown in Fig. 9.f (plotted in red). They show a virtually incompressible response, reaching stress values around 3–4 MPa for a 10% volumetric compression. Upon closer

inspection, we observe that for the physiological hydrostatic pressure range, the volumetric variation is less than 1% (about 0.5% for 30 kPa) for all the contrasted groups. Therefore, we can reasonably assume that the myocardium exhibits an incompressible response.

3.4. Mechanical response post-infarction: Remote regions

Figs. 9.c–f shows the comparison of control animals with non-infarcted remote tissue from LAD and LCX (M-NIT and A-NIT, respectively). The equibiaxial ratio of the Bx results, EBx, show a similar response between the remote tissue, both in LAD and LCX, and the tissue in the physiological state (Figs. 9.c–d). All show similar peak stress values (between 5 and 15 kPa). At the AMFW area (M-C and M-NIT), no significant differences were observed between control and NIT tissue ($p > 0.27$), suggesting that infarction has a local impact on cardiac tissue. We did observe changes between the two contrasting zones (M-C and A-C). As mentioned in [6], we attributed these local differences to changes in fiber orientation in both zones and to the nature of the biaxial test itself. Lastly, there are some visible differences between A-C and A-NIT, being the A-NIT response closer to the M-C results than to A-C. However, the number of samples in A-NIT was very small ($n = 3$), so differences may be due to A-NIT not being a representative sample rather than to changes in tissue physiology in that case. This is in good agreement with the histological results, which highlighted very similar structures between the control groups and the remote non-infarcted tissue.

The STS results show an orthotropic response in all cases. For the 6 individual shear configurations, no differences were observed between control and LCX animals. Regarding LAD results, we observed a similar behavior at FS, SF, and NS, but some differences appear at FN, SN, and SF, being only statistically significant in NF and FN ($p < 0.024$ in both cases). There is no clear justification for that, as we did not observe any irregularity in the NF-FN samples in terms of tissue physiology. Given the complete set of mechanical and histological results, we assume that the differences are not linked to remodeling or changes in tissue structure in the remote zones.

Finally, CC results show highly incompressible behavior in all three groups (control, LAD, and LCX). Minor differences were observed in the compressibility of the three groups, although not significant ($p > 0.24$), suggesting that the tissue also maintains its compressive properties in remote areas to the infarction.

3.5. Mechanical response post-infarction: Infarcted tissue

Fig. 10 compares the EBx Cauchy stress of all the considered groups, including FIT. Focusing on the AAFW results (Fig. 10.a), the A-FIT response shows evident stiffening when compared to the physiological state, obtaining a much more exponential-like and isotropic response. These results correspond to the LAD model, in which severe transmural infarctions were obtained with an important remodeling process in all hearts. As seen in the histological analysis, infarcted tissue exhibited a collagen-dominated structure, which is well related to the observed stiffened response. This collagen arrangement also showed a random fiber orientation in the AAFW region, which explains the isotropic behavior observed under EBx conditions. Lastly, the aforementioned reticulated nature of the collagen fibers is also well related to the increased exponential behavior of the infarcted tissue.

On the other hand, due to the heterogeneous LCX infarctions, samples were divided into transitional tissue, M-TT, locally infarcted tissue, M-LIT, and fully infarcted tissue, M-FIT. The results show progressive stiffening with the degree of infarction associated (Fig. 10.b). First, the M-TT samples showed a comparable response to that of the physiological state, without any visible stiffening when compared to M-C ($p > 0.52$). We did observe significant differences between M-C and M-LIT, especially in CFD ($p = 0.048$ in MFD and $p = 1.3e{-}5$ in CFD). Peak stresses were compared for the statistical analyses. Lastly, similar to the AAFW zone, the M-FIT samples showed an evident severe stiffening. However, M-FIT and A-FIT presented very different responses in terms of anisotropy. A-FIT presented low values of anisotropy, especially in low strain values, where it presented almost an isotropic response. Conversely, M-FIT presented a highly anisotropic response starting at early levels of strain. Furthermore, M-FIT exhibited higher stiffness in the circumferential direction, contrary to A-FIT, where, although more isotropic, the longitudinal direction was the stiffest. This is again related to the microstructural differences observed between both areas, as M-FIT presented a much more preferentially oriented collagen network, which translates into a more anisotropic response. Furthermore, as shown in Fig. 8, the collagen network at M-FIT seemed to follow the circumferential direction. All these results clearly show that the infarction produces a stiffening of the myocardial tissue and that this is proportional to the degree of infarction reached. Moreover, MI has proved to present a very local effect. Lastly, although there is a common trend between LAD and LCX results, differences have been observed between the two in terms of anisotropy.

Once again, it should be noted that, due to the impossibility of cutting laminae in the FIT, its testing directions are not coincident with those of the other groups. In this case, the samples were aligned with the global longitudinal and circumferential directions of the ventricle (shown as LONG and CIRC in different colors in Fig. 10.c, respectively). Therefore, to ensure a more objective comparison between all groups, we chose to obtain the averaged peak stresses between both testing directions for all groups (Fig. 10.d). The averaged results show the same trend as in the previous graphs, confirming the progressive stiffening proportional to the degree of tissue infarction in the M-LIT and M-FIT samples ($p \ll 1e{-}5$ for M-FIT when compared to M-C). If we quantify this stiffening, we observe that the peak average stress reached in M-LIT is 2.19 times the value of the physiological state (M-C), while in the case of M-FIT, this value reaches 4.49 times the original value. In the apical zone, the values reached in A-FIT are 6.26 times higher than the control group ($p \ll 1e{-}5$).

We also examined the variation of cross-coupling effects among the different sample groups (Figs. 11.a–d) using the Cross-Coupling Ratio (CCR). Fig. 11.e summarizes the mean CCR values for each group, and Table 5 provides the corresponding numerical results. No significant variations in CCR were found in non-infarcted tissue samples ($p > 0.05$ in all cases), whether proximal or distal to the infarct (M-NIT, M-TT, and A-NIT), so they were not included. Similar CCR values were also obtained between the two physiological control regions, M-C and A-C (Table 5).

In contrast, infarcted tissues exhibited a markedly amplified CCR, indicating a stronger dependence of the mechanical response on the transversal loading state (Figs. 11.b and d). Once again, although FIT samples do not share the same orientation reference as the remaining groups, the magnitude of the differences observed in CCR is large enough to draw meaningful macroscopic conclusions. Overall, statistical analysis revealed the following: (i) there are no significant differences in CCR between the different zones studied in the physiological state, M-C and A-C ($p > 0.15$ in all ratios). (ii) A-FIT shows significantly larger CCR values than A-C ($p < 0.029$ in all ratios). (iii) Significant variations are observed in both directions for both M-LIT and M-FIT, across all loading ratios ($p < 0.037$ for M-LIT and $p < 0.012$ for M-FIT).

These findings confirm that cross-coupling effects are more pronounced in infarcted tissue samples, indicating a greater interrelationship between testing directions. This correlates well with the collagen fiber distribution observed in the histological study, where collagen fibers are not oriented independently around MFD/CFD but exhibit a three-dimensional distribution that enhances in-plane coupling.

Lastly, we also analyzed the variation in compressive response in LCX compared to the control and remote tissue (Fig. 9.f). Due to the small size of the infarcted area, we could not obtain a large number of compressive samples ($n = 4$). Nevertheless, significant differences

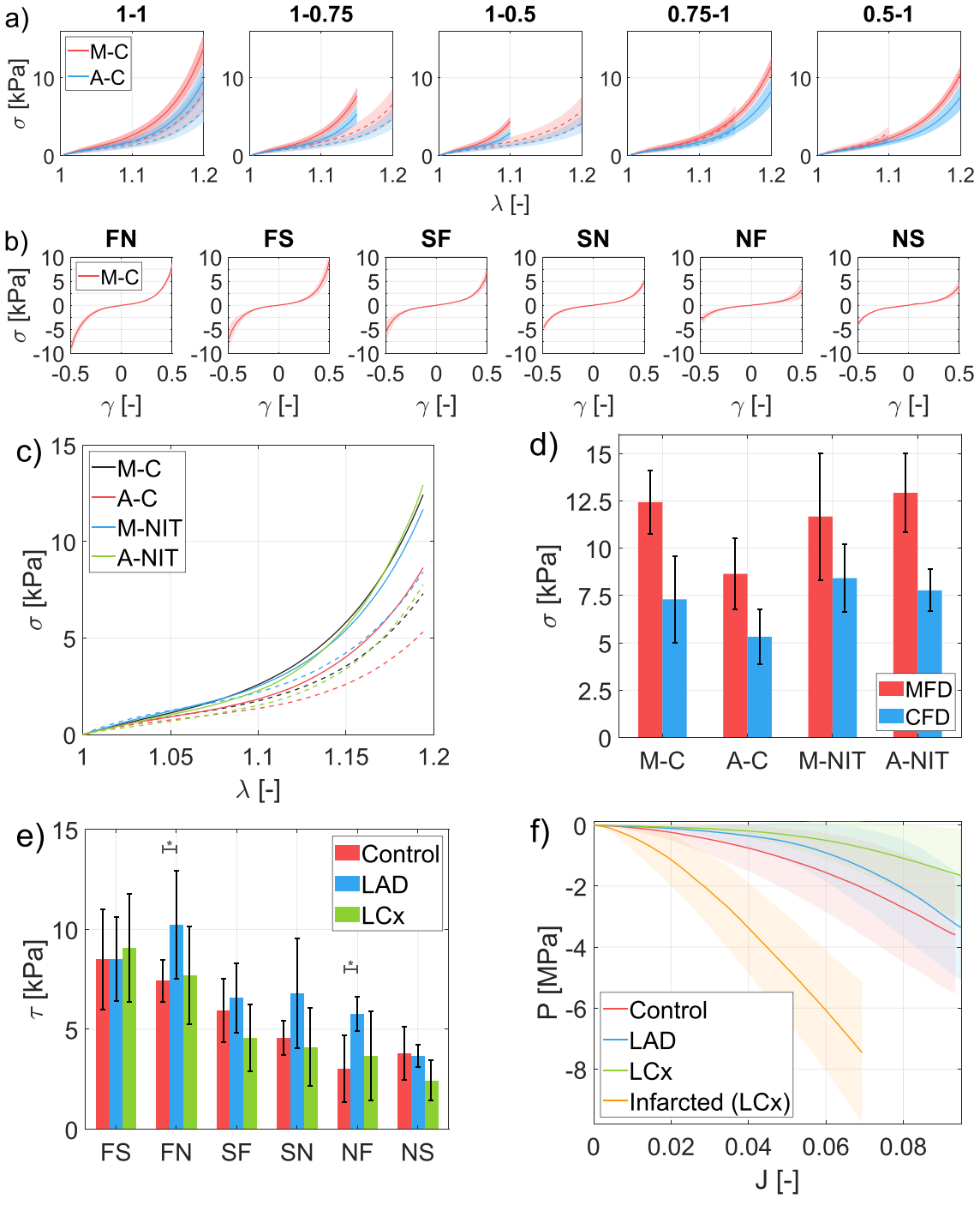

Fig. 9. Healthy and remote-to-infarction tissue results. (a) Bx response for healthy myocardium, both at AMFW (M-C) and AAWF regions (A-C). (b) STS response for medial healthy myocardium (M-C). (c) EBx response at 20% stretch for control vs LCx and LAD remote non-infarcted regions. (d) Averaged peak stress values at 20% stretch for control and non-infarcted biaxial samples. Comparison between control animals and remote, non-infarcted regions in LAD and LCx animals, both for (e) STS and (f) CC. In (a) and (c), solid lines correspond to MFD and dotted lines to CFD. In (e), statistically significant differences ($p < 0.05$) are marked with an asterisk (*).

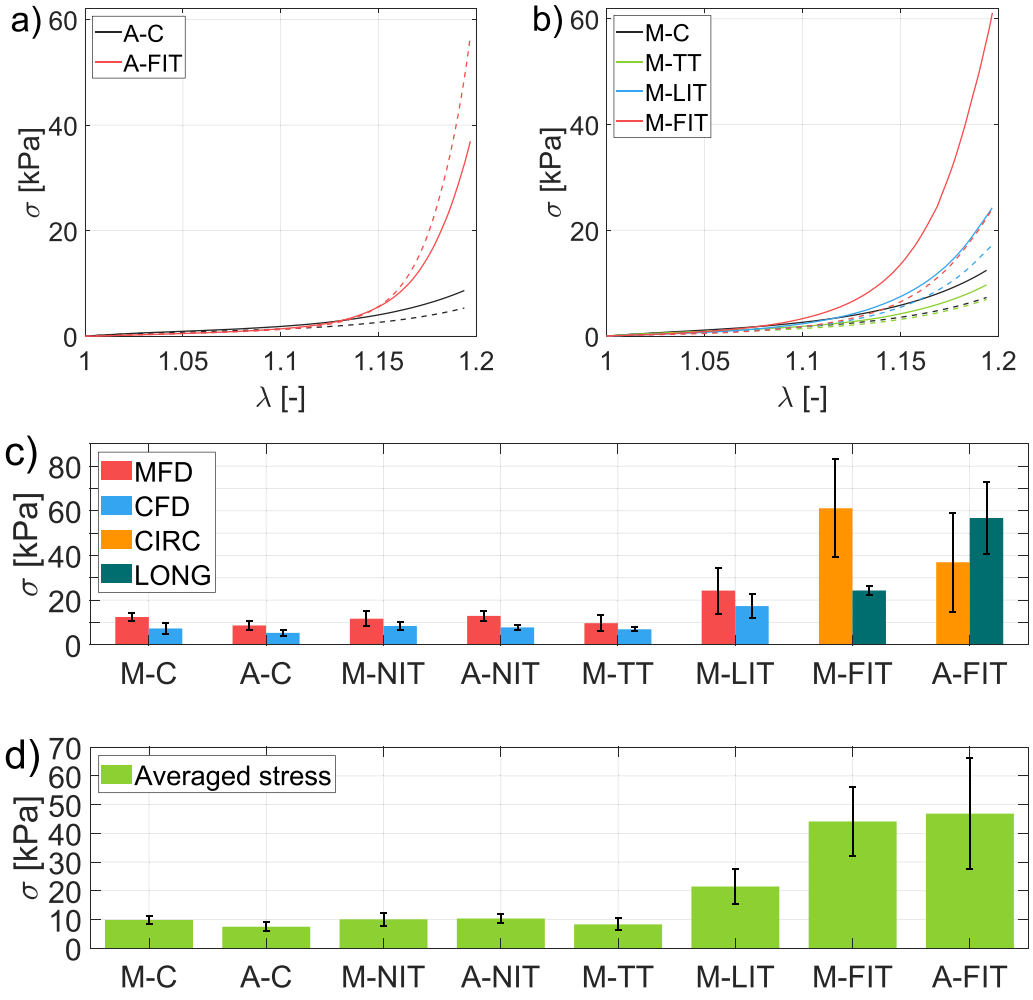

Fig. 10. Infarcted tissue equibiaxial results comparison. (a) Equibiaxial response for all the contrasted groups in AAFW (A-C and A-FIT). (b) Equibiaxial response for all the contrasted groups in AMFW (M-C, M-TT, M-LIT, and M-FIT). (c) Summary of all the peak Cauchy equibiaxial stresses at testing directions for all the contrasted groups. (d) Summary of all the peak Cauchy stress values averaged between testing directions for all the contrasted groups. In plots a–b, solid lines correspond to MFD in all samples except for FIT samples, where they denote global circumferential direction (Circ); similarly, dashed lines correspond to CFD and global longitudinal direction (Long).

Table 5
Cross-coupling ratio for infarcted tissue biaxial testing.

Group	CFD-1:0.75	CFD-1:0.5	MFD-1:0.75	MFD-1:0.5
M-C	17 ± 8%	25 ± 17%	14 ± 4%	23 ± 5%
A-C	20 ± 4%	31 ± 6%	14 ± 4%	21 ± 7%
M-LIT	27 ± 8%	42 ± 12%	18 ± 4%	31 ± 6%
M-FIT	35 ± 4%	54 ± 8%	22 ± 5%	33 ± 7%
A-FIT	31 ± 9%	46 ± 13%	46 ± 4%	65 ± 5%

are evident compared to all control and remote tissue groups (at least $p < 0.0019$ in all cases). The infarcted tissue exhibits notably higher compressive pressure values, even being unable to reach the maximum imposed volumetric variation of 10%. Therefore, the changes occurring in the tissue due to the infarction not only alter its extensive elastic properties but also its compressive ones.

4. Discussion

4.1. Infarcted tissue physiology

We have shown that infarcted hearts differ in morphology and microstructure from control animals. The geometric remodeling process is well known to vary through the infarction healing process, and its process has been extensively reported [14,21,22,26,44]. In our study, we focus on already remodeled tissue, as samples were obtained 6 weeks after the infarction, which is normally considered as so [14]. For LCX hearts, infarctions ranged from mild locally infarcted tissue to transmurally infarcted tissue, the latter affecting up to 20% of the LV wall. For LAD animals, all hearts presented transmurally infarcted tissue, affecting up to 40% of the LV wall. Therefore, LAD infarctions exhibited a greater extent and homogeneity. In the LCX model, it is challenging to generate infarcts as prominent as those in LAD, since its location (AMFW) may compromise the animal's survival until the extraction time (6 weeks later). However, we lack a clear justification for the heterogeneity observed in LCX infarcts, as the same protocol was used in LAD. The authors suggest that this variability may be linked to inter-patient differences in the branching of the LCX artery.

Partially infarcted LCX animals (LCX-1, LCX-3 & LCX-5) did not present any transmural remodeling, maintaining a homogeneous wall thickness similar to control hearts (around 10–15 mm). In contrast, fully infarcted animals, both from LAD and LCX, presented a significant remodeling, with a thickness reduction of about 45%–60% in the infarcted area. This reduction only affected the infarcted area, as the rest of the ventricle maintained a similar thickness to that of the control hearts (Fig. 1 and Table 4).

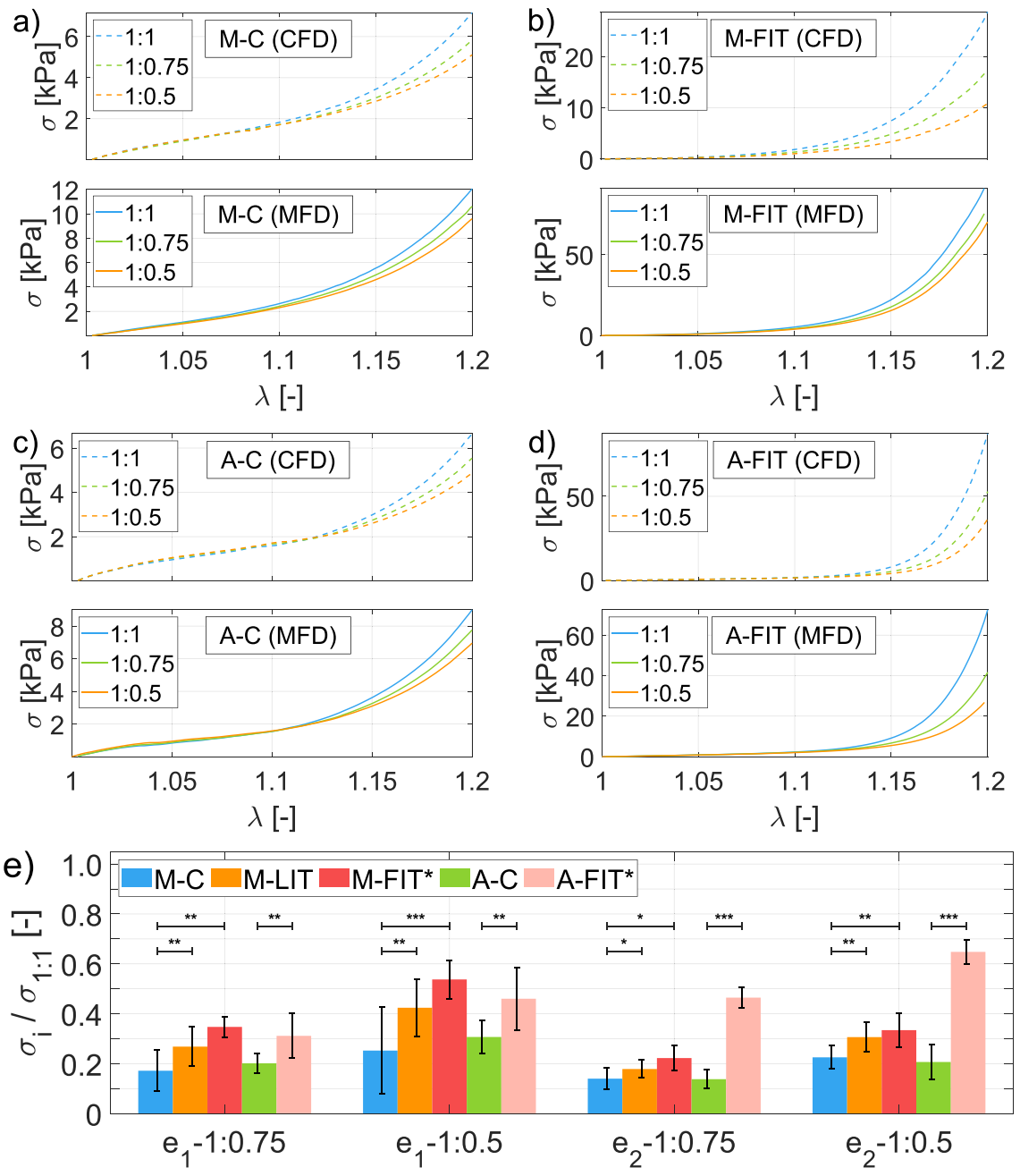

Fig. 11. Biaxial cross-coupling effects. Evolution of the elastic response along the different ratios of the biaxial tests for a representative specimen of (a) M-C, (b) M-FIT, (c) A-C, and (d) A-FIT. CFD is on top, and MFD is on the bottom. (e) Mean Cross-Coupling Ratio, CCR, for all the contrasted groups at the different loading ratios. *e_1 stands for CFD direction in all samples except FIT samples, where it stands for Long direction; e_2 stands for MFD direction in all samples except FIT samples, where it stands for Circ direction. In (e), statistical significance is indicated as $p < 0.05$ (*), $p < 0.01$ (**), and $p < 0.001$ (***).

This aligns with the ranges reported by Richardson et al. [14], who highlighted variations between 20%–60% across different animal models, measurement methods, and times between infarction and results collection [24,26,45–49], although this remodeling process is well-known to be conditioned by tissue reperfusion [50,51]. Gupta et al. [21] examined *in vitro* samples from adult ovine hearts, identifying local remodeling as well, with a 33% reduction in thickness in the infarcted area 6 weeks post-infarction, while physiological thickness was maintained in remote areas. Similarly, McGarvey et al. [22] observed *in vivo* reductions of 30%–55% in porcine hearts between 4 and 8 weeks post-infarction. Although they report slightly lower thickness reductions compared to our findings, they are still comparable. We believe these differences are related to variations in the animal models, as their studies involved younger animals with smaller hearts, which could influence the results.

Regarding the histological microstructure, we have demonstrated distinct patterns in each of the groups analyzed, depending on the degree of infarction of the tissue concerned. Control animals showed a very ordered structure in the M-C samples, alongside a much more random distribution in A-C samples (Fig. 5). Both regions exhibited a very weak collagen network, barely visible under M3 (Fig. 6), but more clearly represented under PR (Fig. 7). Both remote areas, M-NIT and A-NIT as well as M-TT near-infarction area, maintained the physiological structure, as no obvious microstructural changes were observed when compared to M-C or A-C. This suggests once again that the contrasted infarctions have a highly localized effect, confined

to the scarred area. This highly localized effect of infarction is well-documented in the literature, both in experimental [22,43,52] and computational studies, where tissue remote from the infarct is typically considered healthy [25,33,44,53]. Whittaker et al. [43] observed no differences between physiological and infarcted hearts outside the infarction zone, except in a few specimens where tissue variations did not extend more than 1 cm from the infarct. In our study, neither observed significant variations in tissue microstructure even in the adjacent M-TT zone.

Partially infarcted tissue, M-LIT, showed heterogeneous muscle distributions ranging from physiologically-like oriented regions to areas where this orientation was completely or partially disrupted (Fig. 5). This tendency is repeated in the collagenous network (Fig. 6). The scarred tissue clearly showed a great abundance of collagen (Fig. 8.a) as well as necrotic cells. Additionally, we observed alterations in the collagen composition of the non-infarcted regions of the M-LIT samples, with a notable increase in collagen within the cleavage planes (6). M-LIT samples exhibited not only collagen-I fibers but also a minor collagen-III network (<10% of the total collagen) within the infarcted tissue (Fig. 8.b), and the collagen network was organized not only along the muscle fiber direction but also extended transversely, forming a bi-dimensional structure (Fig. 7). The scar composition has been described as primarily consisting of collagen-I, although several studies have also reported the presence of collagen-III, often associated with regions undergoing healing [43,54,55], and even collagen-V [56]. However, collagen-I remains the predominant component of infarcted tissue, being much more abundant than collagen-III, with a reported ratio of 7:1 in mature rats [57]. Whittaker et al. [43] noted that near the edge of the scar, collagen-III fibers form a mesh-like pattern that serves as a scaffold for collagen-I deposition, becoming 'woven' into it. They also observed that in the central part of the scar, this collagen-III structure was less evident, with collagen-I being the primary component. In our case, in both partial and full infarctions, collagen-I was the main component, with a ratio greater than 9:1 in every sample (Fig. 8.a). This may relate to Whittaker's observations, as collagen-III has been associated with tissue still undergoing healing [43], whereas in our case, at six weeks post-MI, the scar may already be sufficiently remodeled.

Lastly, the fully infarcted samples exhibited an intense collagen-I network. Medial samples, M-FIT, presented a clear directionality (Fig. 8.c), forming long collagen chains with a strong circumferential orientation. Collagen fibers showed a prominent reticulated wavy nature. This preferential direction of collagen is aligned with the muscle fibers' direction in the region, suggesting that the collagen network forms following the orthotropic directions of the tissue. In the apical zone, A-FIT, an extensive collagen network was also observed, but here the collagen fibers exhibited a much more random orientation (Fig. 8.d), similar to what we observed about the muscular fibers. Although a greater macroscopic concentration of collagen-III was visually observed in the A-FIT samples, quantitative analysis showed no significant trend, and all infarcts contained less than 10% collagen-III, including the partially infarcted M-LIT samples. It would be of interest to analyze the evolution of both collagen types throughout the scar healing process. The observed collagen fiber distributions in AMFW and AAFW are well related to previous studies of the literature, which agree that fibers are preferentially circumferential in the medial region of the LV and almost randomly distributed in the apical part [18,20,43].

4.2. Healthy cardiac tissue's mechanical response

Healthy myocardium response was extensively analyzed in [6]. Very briefly, the myocardium exhibits a highly non-linear hyperelastic behavior, clearly anisotropic under biaxial conditions and orthotropic under triaxial loading. We obtained a biaxial anisotropy ratio of 2–2.4 and a triaxial orthotropy ratio of 1–0.59-0.41, which aligns well with the literature [2,3,3,4,58–60]. Regarding myocardium compressive properties, a highly incompressible behavior in the perfused state has been demonstrated, which is consistent with the results reported by Avazmohammadi et al. [10] for end-diastole, where the myocardium is also saturated due to coronary perfusion. However, the protocols used in that study and in ours represent two fundamentally different approaches: their work analyzed in vivo volumetric changes during the cardiac cycle due to blood perfusion and at much larger scales, whereas our study involved confined samples tested through in vitro methods. Therefore, this correlation should be interpreted with caution. Still, we believe it is reasonable to conclude that myocardium can be safely considered incompressible under physiological conditions, but only when saturated.

4.3. Remote non-infarcted tissue's mechanical response

We observed similar biaxial responses between control tissue and tissue remote to infarction, both in LAD and LCX (Figs. 9.c–d). We did not observe significant statistical differences between medial control and NIT tissue ($p > 0.27$). There were some visible differences between A-C and A-NIT, but they were attributed to the very reduced number of samples in A-NIT ($n = 3$). This is in good agreement with the histological results, which highlighted very similar structures between the control groups and the remote non-infarcted tissue. The study by Gupta et al. [21] validates our hypothesis, as they also analyzed the response in a remote region of anteroapically infarcted ovine hearts and observed that the equibiaxial properties of the remote tissue had mostly recovered to control levels by a time point comparable to ours (6 weeks). Although numerically, this was also later validated in McGarvey's [22].

The simple triaxial shear results show an orthotropic response in all cases. For LAD animals, we observed relevant differences in peak shear stresses for FN and NF modes when compared to the control. Similar to the control animals (see [6]), we calculated the orthotropy ratios for LAD and LCX, obtaining 1–0.68-0.5 and 1–0.52-0.36, respectively. This translates into a stiffness reduction of 32 and 48% in stiffness from the myocyte direction to the intermediate one, and a reduction of 50 and 64% for the most compliant direction, respectively. This is similar to the contrasted STS studies in healthy tissue (35%–50% and 50%–70%, respectively) [2–4,6]. Therefore, as LAD and LCX results are still around the literature range for physiological STS response and considering the complete set of mechanical and histological results, the authors assume that the observed isolated differences in those STS configurations are not linked to a remodeling process or changes in tissue structure in the remote zones.

Lastly, CC results show highly incompressible behavior in the three groups studied (control, LAD and LCX), with minor non-significant differences between the three groups ($p > 0.24$). This suggests that the tissue also maintains its physiological compressive properties in remote areas. To the best of our knowledge, the compressibility in remote areas from the infarct has not been experimentally characterized to date; thus, there is limited literature available on this topic. The closest study addressing this issue is by Avazmohammadi et al. [10], where they analyzed volumetric variations throughout the cardiac cycle in apically infarcted ovine hearts, specifically recording these variations in remote zones as well (medial and basal). They observed that while the infarcted apical tissue exhibited minimal volumetric changes over the cycle, no such effect was evident in remote zones, maintaining values relatively close to the physiological case. However, this study only focuses on a timeframe of up to 12 h post-infarction, which, as previously mentioned, may not represent the remodeled state typically observed at 6 weeks post-infarction [14,21,22,26,44]. Nevertheless, they also suggest that tissue compressibility in remote infarcted areas may resemble the physiological state.

4.4. Infarcted tissue's mechanical response

4.4.1. Infarcted tissue stiffening

Numerous studies have shown drastic changes in the mechanical properties of post-infarction myocardial tissue. In the early study by Holmes et al. [19], they demonstrated a significant reduction in *in vivo* circumferential systolic deformations for infarcted tissue, suggesting increased stiffness in that direction related to the formation of a prominent collagen network. This has been subsequently validated experimentally [18,20,26] and numerically [25,44].

Focusing on our results, the close-to-infarction tissue, M-TT, presented very similar behavior to that of physiological tissue, confirming that the adjacent tissue maintains its mechanical response, at least from a passive standpoint. This aligns with the conventional approach used in computational studies, which typically considers physiological passive properties in the entire non-infarcted ventricular wall [25,44]. There are indeed studies that considered variations in areas near the MI in terms of active mechanical response [33,53], but that is beyond the scope of our study.

Infarcted tissue showed progressive stiffening depending on the degree of infarction. For M-LIT samples, the increase in the averaged peak stresses compared to the control samples went up to 2.19 times. Similarly, it reached values of 4.49 for M-FIT and 6.26 for A-FIT. Histological analysis revealed that these changes were due to the collagen deposition in the infarcted tissue. We attribute the greater stiffening observed in A-FIT to the larger extent of LAD infarcts, as well as the higher collagen deposition values obtained (Fig. 8.a). In other *in vitro* characterization studies in the literature, such as those by Gupta et al. [21], increases of up to 5.95 times in the circumferential direction compared to the physiological state were observed. In the study by Zhuan et al. [44], although through simulation, circumferential stress increases of about 3.5 times (from 4.3 to 15.1 kPa) were recorded, while longitudinal stresses remained relatively stable.

The study by Gupta et al. [21] reported, for 10% equibiaxial deformation in infarcted samples obtained from the medial region of ovine hearts, mean peak Cauchy stresses of 1.18–0.39 kPa in the circumferential–longitudinal directions. Studies by Morita et al. [24] and Avazmohammadi [5], also on ovine hearts but closer to the apical region, showed values of 10.44–11.11 and 0.64–0.59 kPa, respectively. McGarvey et al. [22] presented simulated values for the medial region of porcine hearts of 7.3–5.2 kPa in the MFD-CFD directions. Zhang et al. [23] presented values of around 8 kPa in the CFD direction in medial samples of porcine hearts. Finally, Sirry et al. [26,27] reported values of up to 20 kPa in both directions for medial samples of murine hearts. All these results correspond to studies of completely infarcted tissue, except for [26], where partially infarcted samples containing about 10 to 70% infarction were obtained. However, that study did not focus on contrasting the impact of partial infarctions vs. total infarctions. In our case, for 10% deformation, we recorded values of 7.99–3.76 and 6.01–6.15 kPa in the circumferential–longitudinal directions of the M-FIT and A-FIT sets, respectively, falling within the literature range.

Therefore, there is a high variability in stresses across all these studies, so special care must be taken when making quantitative comparisons. This significant dispersion, in addition to the inherent variability of biological tissues and differences in testing protocols and animal models, is due to the high complexity of infarct generation methodologies. Inducing infarcts of comparable extent, with precise location and reproducible methodology, is highly complicated. Any subtle change in animal experiences can result in pronounced differences in both the mechanical response and the morphological characteristics of the infarcted tissue [25,26], as seen in our case with M-LIT and M-FIT, despite maintaining the same protocol.

Additionally, all the contrasted studies consider different times between infarct occurrence and data collection, and it has been widely reported that the mechanical response of scarred tissue varies over the first few weeks or even months post-infarction [10,21,22,44]. The available studies present very different conditions, so caution must be exercised when comparing them. Nevertheless, a clear trend of myocardial tissue stiffening at the latter stages post-MI, dependent on the extent of infarction and the microstructural composition of the scar, is observed across all studies, which aligns with our results.

4.4.2. Infarcted tissue anisotropy

In addition to becoming stiffer, it is well known that the mechanical response of infarcted tissue is highly influenced by its location and the deformation state to which it is subjected. The study by Zimmerman et al. [29] was the first to report that local changes in the strain conditions influenced the microstructure of the scar. This was later corroborated by Fomovsky et al. [20], who found that apical infarcts exhibited more isotropic properties compared to medial ones. In a subsequent study [18], they contrasted infarcts of different geometries and locations, comparing the medial and apical regions. They found that only infarct location affected its mechanical response: medial infarctions stretched primarily in the circumferential direction and developed anisotropic scars containing circumferentially aligned collagen fibers, while the apical ones stretched in both the circumferential and longitudinal directions, developing structurally isotropic scars. These mechanical responses are justified by tissue microstructure as the collagen network was coincident with those descriptions. All this suggests that the mechanical conditions surrounding the infarct dominate the scar development process and determine its final properties. This mechano-dependent nature of collagen deposition aligns with the results of other experimental studies [5,21,23,24,26] and has also been validated numerically [44]. Additionally, this trend has been reported in studies on other tissues as well [61–63].

In our results, transmural medial infarcts (M-FIT) exhibited an anisotropic response with significantly greater stiffness in the circumferential direction, consistent with previous studies [18,23,25,26]. This was corroborated by histological analysis, which revealed a dense network of collagen fibers aligned in this direction. On the other hand, A-FIT samples showed a much more isotropic response, especially up to deformations of approximately 15%. Once again, the microstructure supported this response, displaying more dispersed fiber patterns than in the medial region, which aligns well with the distributions presented by Fomovsky et al. (see Figure 3 of [18]).

Lastly, partial medial infarcts, M-LIT, exhibited increased stiffness compared to the physiological state, but we did not find differences in terms of anisotropy. The histological study revealed various microstructural patterns, finding infarcted areas where the fibers were parallel to the muscle structure and others where the orientation was more dispersed. We also noted an increase in 'perimysial' collagen in the cleavage planes in non-infarcted areas. This suggests that these heterogeneous distributions do not generate a uniform effect on tissue anisotropy and depend greatly on inter-patient variability and the specific conditions of each infarct.

Considering the computational application of the experimental data collected, especially since we observed significant differences in the mechanical responses of M-FIT and M-LIT, it is important to move towards patient-specific models that can incorporate specific information about the type and extent of the infarct, as this may have major implications on the simulated results. In the recent study by Martonová et al. [25], a modified material model was proposed that allows the inclusion of the degree of infarction in its formulation, opening the door to the consideration of experimental data, as the one we propose. We believe that such approaches can benefit from the data presented and facilitate moving towards increasingly realistic patient-specific models that can improve the development of new personalized therapies.

4.4.3. Infarcted tissue biaxial in-plane coupling

All sample groups presented different levels of cross-coupling effects at the non-equibiaxial testing. We observe no significant differences in CCR between the different zones ($p > 0.05$) where the tissue was considered to remain in the physiological state (M-C, A-C, M-NIT, A-NIT, M-TT).

In the infarcted samples, these differences increased gradually (M-LIT<M-FIT<A-FIT). This is consistent with the findings of [26], where they also quantified in-plane coupling, recording higher values in samples with a more prominent scar (28d animals). The exact underlying mechanism causing this phenomenon is not clear, though some hypotheses attribute it to the dynamic change of collagen orientation in response to unequal biaxial loading [64–66]. In the medial samples, M-LIT and M-FIT, the increases in CCR were more pronounced in the CFD-Long directions, which proved to be mechanically weaker in the mechanical tests. A-FIT samples also showed the highest variations in the Circ direction, which was also the weakest direction in the mechanical tests. We do not have a clear justification for this relationship, so further analysis would be needed to draw solid conclusions. Additionally, the significant increase in CCR for the Circ direction in A-FIT samples (reaching values of 46% and 65%, respectively) is noteworthy, marking the most drastic difference among all groups. This relates to their microstructure observed in the histological analysis, which revealed a highly irregular fiber distribution and a high presence of collagen, promoting these elevated cross-coupling effects. In light of all these results, we believe there is a clear correlation between the structural changes induced by the infarction and the in-plane coupling. This implies that the infarcted tissue presents more intricate structures than the well-organized and directionalized architecture of physiological cardiac tissue.

4.4.4. Infarcted tissue compressive response

Lastly, higher compressive pressures were obtained in infarcted tissue than in the remote non-infarcted regions or the control animals. This again correlates to the results of [10], where they also recorded a reduction in the *in vivo* end-systolic volumetric variation at 12 h post-MI when compared to the physiological state. This was also reported in Sirry et al. [26,27], where they recorded an increase in the compressive stiffness of 4 weeks post-MI tissue. However, the considered times after infarction in these studies do not correspond with ours (6 weeks post-MI).

4.5. Mechanical implications of the characterized infarcted response

After extensive analysis of myocardial tissue in both physiological and infarcted stages under two of the most common infarction models, LCx and LAD, we have confirmed that infarction induces irreversible structural changes in the tissue that alter its mechanical response.

Our results also demonstrate that infarcted tissue is stiffer than physiological tissue, showing a strong correlation between the degree of infarction and the mechanical properties of the myocardium. Infarcted samples exhibited greater in-plane coupling between anisotropic directions compared to healthy tissue, reflecting a more complex and crosslinked microstructure. They also displayed increased compressive resistance. These changes in mechanical response can be explained by the microstructural alterations observed histologically and were restricted to the scarred area, as adjacent and remote tissues preserved physiological characteristics.

Additionally, we observed that LCX and LAD models produce scars with distinct mechanical behaviors. It is important to emphasize the differences between the MI models, which may otherwise appear diluted due to the heterogeneous degrees of infarction observed in the LCX model. Despite this variability, our results clearly distinguish the two models. Fully infarcted medial (LCX) samples exhibited a pronounced anisotropic response, with collagen fibers predominantly aligned along the global circumferential direction of the ventricle. Histology revealed a marked increase in collagen, distributed relatively homogeneously along this direction (Fig. 8.c), leading to tissue stiffening. In this case, average tensile peak stresses reached approximately 4.5 times those of healthy tissue. The scar was mainly composed of collagen I (Fig. 8.b). Conversely, apical (LAD) infarcts showed a much more isotropic mechanical response, lacking a clear preferential direction. Histological analysis again revealed a marked collagen increase, significantly higher than in LCX infarcts. Here, the newly deposited collagen fibers displayed a clearly random distribution (Fig. 8.d). Average tensile stresses reached values around 6 times greater than physiological levels, consistent with the higher collagen content. The scar was also predominantly collagen I, with no relevant differences compared to LCX in this aspect.

Overall, both models led to collagen accumulation and consequent tissue stiffening. However, LAD infarcts exhibited greater collagen content and extent, resulting in more pronounced stiffening than LCX infarcts. In addition, the contrasting collagen fiber organization (directional in LCX versus random in LAD) produced substantial differences in anisotropy between the two models.

To our knowledge, no other *in vitro* experimental study has been as comprehensive as ours, as is the first that jointly: (i) compares two prevalent MI models (LAD vs LCX) under a standardized protocol; (ii) contrasts transmural and localized (partial) infarcts; and (iii) integrates multimodal mechanics (biaxial, simple triaxial shear extension and confined compression) with quantitative histology. Our findings establish mechanical correlations between collagen architecture and myocardial mechanics across infarct types, locations, and extents, providing data directly translatable to computational modeling and therapy design. Lastly, this study also builds upon our previous, equally extensive analysis of healthy myocardium [6], providing a coherent and complementary framework to understand the transition from normal to post-infarction mechanical behavior.

Sirry et al. [26] likely represents the previous most extensive experimental work, analyzing both extensional and compressive properties of infarcted tissue; however, it does not examine variation across infarcted, adjacent, and remote regions, nor does it compare different prevalent MI models. Previously, the only data comparing MI models came from Fomovsky et al. [18], based on a murine in vivo model that is less comparable to the human heart.

Beyond quantifying the full three-dimensional mechanical response for all groups, we show that infarcted tissue behavior varies markedly with location and, critically, with infarct extent. Focusing on localized versus transmural infarcts, we observed substantial differences in both mechanical response and remodeling. These findings have significant implications for cardiac physiology [25]. To enable reliable computational models and more effective therapies, it is essential to account for such heterogeneities and to move toward personalized studies encompassing a wider and more realistic range of cases.

4.6. Limitations

Some limitations in this study need to be highlighted. Firstly, the *in vitro* tests may compromise the physiological behavior of the tissue due to potential damage, resulting in the fact that subsequent results could be unrepresentative of *in vivo* behavior [67,68].

Again, the loss of tissue's physiological state was a clear limitation, as tests could not be extended more than 72 h after extraction. Consequently, we were unable to perform all types of tests simultaneously at every location in all animals. This resulted in some groups being limited to a few samples, such as A-NIT ($n = 3$). Furthermore, in addition to these temporal limitations, we also faced significant spatial constraints in infarcted samples. The infarcted area generated in the ventricular free wall was about 20–25 mm maximum, which considerably limited the number of tests that could be performed on the infarcted tissue. For example, we were unable to evaluate the infarcted tissue under STS.

Obtaining homogeneous and reproducible infarcts in all animals also posed a considerable challenge. Ensuring an objective comparison,

both with our results and with those in the literature, requires meticulous control of many factors that can introduce variability [25,26]. Even small changes in the infarction model, the arterial occlusion protocol, or the time between infarction and data collection can lead to marked differences in scar microstructure, geometric remodeling, and mechanical response. For instance, in our study, a 90-minute reperfusion period was applied after MI in both LCX and LAD models, whereas most tissue characterization studies referenced in Table 1 employed permanent coronary ligation, except Zhang et al. [23]. This difference may partly explain the heterogeneity observed in LCX infarcts; however, the same reperfusion protocol did not cause variability among LAD infarcts, which remained fully homogeneous. Furthermore, studies such as Sirry et al. [26] also reported partial infarcts despite using permanent ligation. Therefore, we believe reperfusion alone cannot fully account for the differences observed, particularly between LCX and LAD infarcts. Future work directly comparing reperfused and non-reperfused samples could help clarify these findings. Ultimately, comprehensive studies covering different infarction models and conditions are needed to better understand the intrinsic heterogeneity of myocardial injury.

Additionally, certain simplifications were made in this study. In all tests, we have assumed a homogeneous macroscopic fiber distribution for stress calculations. However, this assumption is only true at the micrometric scale (250–500 μm) and disregards the tissue dispersion and heterogeneities. Due to the heterogeneity of test loading conditions and cardiac tissue structure, finite element modeling would be highly beneficial to validate and corroborate our three-dimensional characterization in a realistic and personalized manner at the microstructural level. Similar to the healthy tissue, both microstructural [5,10,28] and macroscopic [21,25,26] approaches have been reported. However, a more detailed microstructural study based on inverse FEM analysis may better capture the infarcted tissue response and could be a valuable direction for future work.

5. Conclusions

We have conducted a comprehensive *in vitro* experimental characterization of infarcted porcine cardiac tissue. Although our analysis focused primarily on biaxial testing (Bx), we also incorporated other relevant deformation modes, including simple triaxial shear tests (STS) and confined compression tests (CC). Furthermore, we explored how mechanical behavior varies across two prevalent infarction models (LAD and LCX) and across different degrees of infarction.

Our results show that non-infarcted tissue, both in areas remote and adjacent to the infarction (for both LAD and LCX models), does not differ significantly from control myocardium, suggesting that infarction induces localized changes in mechanical properties.

In contrast, infarcted tissue exhibited markedly increased stiffness compared with non-infarcted myocardium, proportional to the infarction extent. Partially infarcted samples showed a less pronounced stiffening (around 2.2 times physiological values) than fully transmural infarcts (about 4.5 times for LCX and 6.3 times for LAD). Hearts with complete transmural infarction experienced a 60% reduction in ventricular wall thickness in the affected area, while localized non-transmural infarcts did not. Infarcted tissue also presented greater in-plane coupling, indicating a more interconnected and complex fiber architecture, which was both extent- and direction-dependent. The LAD model produced more extensive infarcts than LCX, resulting in a stiffer and more isotropic mechanical response. Histological analysis corroborated these mechanical findings, revealing distinct remodeling of muscle and collagen structure underlying the observed mechanical differences. Tissue architecture was predominantly shaped by infarction location and the associated local strain environment.

To our knowledge, this work provides the most detailed *in vitro* mechanical and histological characterization of post-infarction myocardium available to date, capturing key heterogeneities that have not been systematically addressed before. In addition, we provide a comprehensive experimental dataset covering all tested conditions, which is rarely available in the current literature and is useful as a reference for future modeling and experimental work. These contributions advance the understanding of myocardial remodeling and provide robust data to refine biomechanical simulations and guide the development of targeted therapeutic strategies.

CRediT authorship contribution statement

Nicolás Laita: Writing – original draft, Visualization, Validation, Software, Resources, Methodology, Investigation, Formal analysis, Data curation, Conceptualization. **Alejandro Aparici-Gil:** Resources, Methodology, Investigation, Data curation. **Aida Oliván-Viguera:** Resources, Investigation, Data curation. **Alba Pérez-Martínez:** Resources, Investigation, Data curation. **Ming Wu:** Supervision, Resources, Investigation. **Manuel García de Yébenes:** Resources, Investigation. **Gloria Abizanda:** Resources, Investigation. **Stephan Janssens:** Supervision, Resources, Investigation. **Felipe Prósper:** Validation, Supervision, Project administration, Funding acquisition. **Manuel M. Mazo Vega:** Writing – review & editing, Validation, Supervision, Project administration, Funding acquisition, Conceptualization. **Miguel Ángel Martínez:** Writing – review & editing, Validation, Supervision, Methodology, Investigation. **Manuel Doblaré:** Writing – review & editing, Validation, Supervision, Project administration, Methodology, Investigation, Conceptualization. **Estefanía Peña:** Writing – review & editing, Validation, Supervision, Project administration, Methodology, Investigation, Conceptualization.

Declaration of competing interest

The authors declare that they have no known competing financial interests or personal relationships that could have appeared to influence the work reported in this paper.

Acknowledgments

This work is supported by the European Union's Horizon 2020 research and innovation programme under grant agreement 874827 (research project BRAV3, C1-BHC-07-2019, H2020); Ministerio de Ciencia y Universidades CARDIOPRINT (PLEC2021-008127), VOLVAD (PID2022-142562OB-I00) funded by MICIU/AEI /10.13039/501100011033 and by the European Union Next Generation EU/PRTR; the Spanish Ministry of Economy and Competitiveness through research project PID2022-140219OB-I00 and the regional Government of Aragón support for the funding of the research project T24-20R. The authors gratefully acknowledge research support from the ICTS, Spain "NANBIOSIS", specifically by the Tissue & Scaffold Characterization Unit (U13) of the CIBER in Bioengineering, Biomaterials & Nanomedicine (CIBER-BBN at the University of Zaragoza). The Instituto de Salud Carlos III finances CIBER Actions with assistance from the European Regional Development Fund. The authors thank the Cardiac Tissue Engineering Group at CIMA for their support with the animal procedures. Authors would also like to gratefully thank our laboratory technician, C. Marzo, as well as C. Laita for his help in the figures layout. The authors also thank the Central Anatomical Pathology Unit and the Experimental Surgery Service of the Aragon Health Sciences Institute.

Appendix. Supplementary data

The control animal data used in this study were originally presented in [6]. These control datasets are publicly available at: https://doi.org/10.5281/zenodo.12706383.

The dataset corresponding to the infarcted animals generated for the present work is available at: https://doi.org/10.5281/zenodo.17688588.

References

[1] I.J. LeGrice, B. Smaill, L. Chai, S. Edgar, J. Gavin, P.J. Hunter, Laminar structure of the heart: ventricular myocyte arrangement and connective tissue architecture in the dog, Am. J. Physiol.-Heart Circ. Physiol. 269 (2) (1995) H571–H582, http://dx.doi.org/10.1152/ajpheart.1995.269.2.H571.

[2] S. Dokos, B.H. Smaill, A.A. Young, I.J. LeGrice, Shear properties of passive ventricular myocardium, Am. J. Physiol.-Heart Circ. Physiol. 283 (6) (2002) H2650–H2659, http://dx.doi.org/10.1152/ajpheart.00111.2002.

[3] G. Sommer, A.J. Schriefl, M. Andrä, M. Sacherer, C. Viertler, H. Wolinski, G.A. Holzapfel, Biomechanical properties and microstructure of human ventricular myocardium, Acta Biomater. 24 (2015) 172–192, http://dx.doi.org/10.1016/j.actbio.2015.06.031.

[4] S. Kakaletsis, W.D. Meador, M. Mathur, G.P. Sugerman, T. Jazwiec, M. Malinowski, E. Lejeune, T.A. Timek, M.K. Rausch, Right ventricular myocardial mechanics: multi-modal deformation, microstructure, modeling, and comparison to the left ventricle, Acta Biomater. 123 (2021) 154–166, http://dx.doi.org/10.1016/j.actbio.2020.12.006.

[5] R. Avazmohammadi, D.S. Li, T. Leahy, E. Shih, J.S. Soares, J.H. Gorman, R.C. Gorman, M.S. Sacks, An integrated inverse model-experimental approach to determine soft tissue three-dimensional constitutive parameters: application to post-infarcted myocardium, Biomech. Model. Mechanobiol. 17 (1) (2018) 31–53, http://dx.doi.org/10.1007/s10237-017-0943-1.

[6] N. Laita, A. Aparici-Gil, A. Oliván-Viguera, A. Pérez-Martínez, M.Á. Martínez, M. Doblaré, E. Peña, A comprehensive experimental analysis of the local passive response across the healthy porcine left ventricle, Acta Biomater. 187 (2024) 261–277, http://dx.doi.org/10.1016/j.actbio.2024.08.028.

[7] J.S. Soares, D.S. Li, E. Lai, J.H. Gorman III, R.C. Gorman, M.S. Sacks, Modeling of myocardium compressibility and its impact in computational simulations of the healthy and infarcted heart, in: Functional Imaging and Modelling of the Heart: 9th International Conference, FIMH 2017, Toronto, on, Canada, June 11–13, 2017, Proceedings 9, Springer, 2017, pp. 493–501, http://dx.doi.org/10.1007/978-3-319-59448-447.

[8] H. Ashikaga, B.A. Coppola, K.G. Yamazaki, F.J. Villarreal, J.H. Omens, J.W. Covell, Changes in regional myocardial volume during the cardiac cycle: implications for transmural blood flow and cardiac structure, Am. J. Physiol.-Heart Circ. Physiol. 295 (2) (2008) H610–H618, http://dx.doi.org/10.1152/ajpheart.00107.2008.

[9] E. McEvoy, G.A. Holzapfel, P. McGarry, Compressibility and anisotropy of the ventricular myocardium: experimental analysis and microstructural modeling, J. Biomech. Eng. 140 (8) (2018) 081004, http://dx.doi.org/10.1115/1.4039947.

[10] R. Avazmohammadi, J.S. Soares, D.S. Li, T. Eperjesi, J. Pilla, R.C. Gorman, M.S. Sacks, On the in vivo systolic compressibility of left ventricular free wall myocardium in the normal and infarcted heart, J. Biomech. 107 (2020) 109767, http://dx.doi.org/10.1016/j.jbiomech.2020.109767.

[11] H. Liu, J.S. Soares, J. Walmsley, D.S. Li, S. Raut, R. Avazmohammadi, P. Iaizzo, M. Palmer, J.H. Gorman, R.C. Gorman, M.S. Sacks, The impact of myocardial compressibility on organ-level simulations of the normal and infarcted heart, Sci. Rep. 11 (1) (2021) 1–15, http://dx.doi.org/10.1038/s41598-021-92810-y.

[12] W. Zhang, J. Jilberto, G. Sommer, M.S. Sacks, G.A. Holzapfel, D.A. Nordsletten, Simulating hyperelasticity and fractional viscoelasticity in the human heart, Comput. Methods Appl. Mech. Engrg. 411 (2023) 116048, http://dx.doi.org/10.1016/j.cma.2023.116048.

[13] J.W. Holmes, T.K. Borg, J.W. Covell, Structure and mechanics of healing myocardial infarcts, Annu. Rev. Biomed. Eng. 7 (2005) 223–253, http://dx.doi.org/10.1146/annurev.bioeng.7.060804.100453.

[14] W.J. Richardson, S.A. Clarke, T.A. Quinn, J.W. Holmes, Physiological implications of myocardial scar structure, Compr. Physiol. 5 (4) (2015) 1877–1909, http://dx.doi.org/10.1002/cphy.c140067.

[15] K. Sunagawa, W.L. Maughan, K. Sagawa, Effect of regional ischemia on the left ventricular end-systolic pressure-volume relationship of isolated canine hearts, Circ. Res. 52 (1983) 170–178, http://dx.doi.org/10.1161/01.RES.52.2.170.

[16] P.J. Fletcher, J.M. Pfeffer, M.A. Pfeffer, E. Braunwald, Left ventricular diastolic pressure-volume relations in rats with healed myocardial infarction. Effects on systolic function, Circ. Res. 49 (1981) 618–626, http://dx.doi.org/10.1161/01.RES.49.3.618.

[17] D.L. Page, J.B. Caulfield, J.A. Kastor, R.W. DeSanctis, C.A. Sanders, Myocardial changes associated with cardiogenic shock, N. Engl. J. Med. 285 (1971) 133–137, http://dx.doi.org/10.1056/NEJM197107152850301.

[18] G.M. Fomovsky, A.D. Rouillard, J.W. Holmes, Regional mechanics determine collagen fiber structure in healing myocardial infarcts, J. Mol. Cell. Cardiol. 52 (5) (2012) 1083–1090, http://dx.doi.org/10.1016/j.yjmcc.2012.02.012.

[19] J.W. Holmes, J.A. Nuñez, J.W. Covell, Functional implications of myocardial scar structure, Am. J. Physiol.-Heart Circ. Physiol. 272 (5) (1997) H2123–H2130, http://dx.doi.org/10.1152/ajpheart.1997.272.5.H2123.

[20] G.M. Fomovsky, J.W. Holmes, Evolution of scar structure, mechanics, and ventricular function after myocardial infarction in the rat, Am. J. Physiol.-Heart Circ. Physiol. 298 (1) (2010) H221–H228, http://dx.doi.org/10.1152/ajpheart.00495.2009.

[21] K.B. Gupta, M.B. Ratcliffe, M.A. Fallert, L.H. Edmunds Jr., D.K. Bogen, Changes in passive mechanical stiffness of myocardial tissue with aneurysm formation, Circulation 89 (5) (1994) 2315–2326, http://dx.doi.org/10.1161/01.CIR.89.5.2315.

[22] J.R. McGarvey, D. Mojsejenko, S.M. Dorsey, A. Nikou, J.A. Burdick, J.H. Gorman III, B.M. Jackson, J.J. Pilla, R.C. Gorman, J.F. Wenk, Temporal changes in infarct material properties: an in vivo assessment using magnetic resonance imaging and finite element simulations, Ann. Thorac. Surg. 100 (2) (2015) 582–589, http://dx.doi.org/10.1016/j.athoracsur.2015.03.015.

[23] S. Zhang, J.A. Crow, X. Yang, J. Chen, A. Borazjani, K.B. Mullins, W. Chen, R.C. Cooper, R.M. McLaughlin, J. Liao, The correlation of 3D DT-MRI fiber disruption with structural and mechanical degeneration in porcine myocardium, Ann. Biomed. Eng. 38 (2010) 3084–3095, http://dx.doi.org/10.1007/s10439-010-0073-8.

[24] M. Morita, C.E. Eckert, K. Matsuzaki, M. Noma, L.P. Ryan, J.A. Burdick, B.M. Jackson, J.H. Gorman III, M.S. Sacks, R.C. Gorman, Modification of infarct material properties limits adverse ventricular remodeling, Ann. Thorac. Surg. 92 (2) (2011) 617–624, http://dx.doi.org/10.1016/j.athoracsur.2011.04.051.

[25] D. Martonová, M. Alkassar, J. Seufert, D. Holz, M.T. Duong, B. Reischl, O. Friedrich, S. Leyendecker, Passive mechanical properties in healthy and infarcted rat left ventricle characterised via a mixture model, J. Mech. Behav. Biomed. Mater. 119 (2021) 104430, http://dx.doi.org/10.1016/j.jmbbm.2021.104430.

[26] M.S. Sirry, J.R. Butler, S.S. Patnaik, B. Brazile, R. Bertucci, A. Claude, R. McLaughlin, N.H. Davies, J. Liao, T. Franz, Characterisation of the mechanical properties of infarcted myocardium in the rat under biaxial tension and uniaxial compression, J. Mech. Behav. Biomed. Mater. 63 (2016) 252–264, http://dx.doi.org/10.1016/j.jmbbm.2016.06.029.

[27] M.S. Sirry, J.R. Butler, S.S. Patnaik, B. Brazile, R. Bertucci, A. Claude, R. McLaughlin, N.H. Davies, J. Liao, T. Franz, Infarcted rat myocardium: Data from biaxial tensile and uniaxial compressive testing and analysis of collagen fibre orientation, Data Brief 8 (2016) 1338–1343, http://dx.doi.org/10.1016/j.dib.2016.08.005.

[28] E.A. Mendiola, S. Neelakantan, Q. Xiang, S. Xia, J. Zhang, V. Serpooshan, P. Vanderslice, R. Avazmohammadi, An image-driven micromechanical approach to characterize multiscale remodeling in infarcted myocardium, Acta Biomater. 173 (2024) 109–122, http://dx.doi.org/10.1016/j.actbio.2023.10.027.

[29] S.D. Zimmerman, W.J. Karlon, J.W. Holmes, J.H. Omens, J.W. Covell, Structural and mechanical factors influencing infarct scar collagen organization, Am. J. Physiol.-Heart Circ. Physiol. 278 (1) (2000) H194–H200, http://dx.doi.org/10.1152/ajpheart.2000.278.1.H194.

[30] H. Gao, K. Mangion, D. Carrick, D. Husmeier, X. Luo, C. Berry, Estimating prognosis in patients with acute myocardial infarction using personalized computational heart models, Sci. Rep. 7 (2017) http://dx.doi.org/10.1038/s41598-017-13635-2.

[31] G. Balaban, H. Finsberg, S. Funke, T.F.H. aland, E. Hopp, J. Sundnes, S. Wall, M.E. Rognes, In vivo estimation of elastic heterogeneity in an infarcted human heart, Biomech. Model. Mechanobiol. 17 (5) (2018) 1317–1329, http://dx.doi.org/10.1007/s10237-018-1028-5.

[32] Y. Zhang, V.Y. Wang, A.E. Morgan, J. Kim, L. Ge, J.M. Guccione, J.W. Weinsaft, M.B. Ratcliffe, A novel MRI-based finite element modeling method for calculation of myocardial ischemia effect in patients with functional mitral regurgitation, Front. Physiol. 11 (2020) 158, http://dx.doi.org/10.3389/fphys.2020.00158.

[33] K. Janssens, M. Kraamer, L. Barbarotta, P.H. Bovendeerd, Post-infarct evolution of ventricular and myocardial function, Biomech. Model. Mechanobiol. 22 (6) (2023) 1815–1828, http://dx.doi.org/10.1007/s10237-023-01734-1.

[34] W. Li, Biomechanics of infarcted left Ventricle-A review of experiments, J. Mech. Behav. Biomed. Mater. 103 (2020) 103591, http://dx.doi.org/10.1016/j.jmbbm.2019.103591.

[35] J.H. Bracamonte, S.K. Saunders, J.S. Wilson, U.T. Truong, J.S. Soares, Patient-specific inverse modeling of in vivo cardiovascular mechanics with medical image-derived kinematics as input data: Concepts, methods, and applications, Appl. Sci. 12 (8) (2022) 3954, http://dx.doi.org/10.3390/app12083954.

[36] A. Oliván-Viguera, M. Pérez-Zabalza, L. García-Mendívil, K.A. Mountris, S. Orós-Rodrigo, E. Ramos-Marquès, J.M. Vallejo-Gil, P.C. Fresneda-Roldán, J. Fañanás-Mastral, M. Vázquez-Sancho, M. Matamala-Adell, F. Sorribas-Berjón, J. André Bellido-Morales, F.J. Mancebón-Sierra, A.S. Vaca-Núñez, C. Ballester-Cuenca, M.Á. Marigil, C. Pastor, L. Ordovás, R. Köhler, E. Diez, E. Pueyo, Minimally invasive system to reliably characterize ventricular electrophysiology from living donors, Sci. Rep. 10 (1) (2020) 1–13, http://dx.doi.org/10.1038/s41598-020-77076-0.

[37] Q. Ou, R.R. Abouleisa, X.-L. Tang, H.R. Juhardeen, M.H. Meki, J.M. Miller, G. Giridharan, A. El-Baz, R. Bolli, T.M. Mohamed, Slicing and culturing pig hearts under physiological conditions, JoVE (J. Vis. Exp.) 1 (157) (2020) e60913, http://dx.doi.org/10.3791/60913.

[38] S.A. Watson, M. Scigliano, I. Bardi, R. Ascione, C.M. Terracciano, F. Perbellini, Preparation of viable adult ventricular myocardial slices from large and small mammals, Nat. Protoc. 12 (12) (2017) 2623–2639, http://dx.doi.org/10.1038/nprot.2017.139.

[39] G. Plank, R.A. Burton, P. Hales, M. Bishop, T. Mansoori, M.O. Bernabeu, A. Garny, A.J. Prassl, C. Bollensdorff, F. Mason, F. Mahmood, B. Rodriguez, V. Grau, J.E. Schneider, D. Gavaghan, P. Kohl, Generation of histoanatomically representative models of the individual heart: tools and application, Philos. Trans. R. Soc. A: Math. Phys. Eng. Sci. 367 (1896) (2009) 2257–2292, http://dx.doi.org/10.1098/rsta.2009.0056.

[40] R.S. Stephenson, A. Atkinson, P. Kottas, F. Perde, F. Jafarzadeh, M. Bateman, P.A. Iaizzo, J. Zhao, H. Zhang, R.H. Anderson, J.C. Jarvis, H. Dobrzynski, High resolution 3-dimensional imaging of the human cardiac conduction system from microanatomy to mathematical modeling, Sci. Rep. 7 (1) (2017) 1–13, http://dx.doi.org/10.1038/s41598-017-07694-8.

[41] G. Sommer, D.C. Haspinger, M. Andrä, M. Sacherer, C. Viertler, P. Regitnig, G.A. Holzapfel, Quantification of shear deformations and corresponding stresses in the biaxially tested human myocardium, Ann. Biomed. Eng. 43 (10) (2015) 2334–2348, http://dx.doi.org/10.1007/s10439-015-1281-z.

[42] R. Rezakhaniha, A. Agianniotis, J.T.C. Schrauwen, A. Griffa, D. Sage, C.V.C. Bouten, F.N. van de Vosse, M. Unser, N. Stergiopulos, Experimental investigation of collagen waviness and orientation in the arterial adventitia using confocal laser scanning microscopy, Biomech. Model. Mechanobiol. 11 (3–4) (2012) 461–473, http://dx.doi.org/10.1007/s10237-011-0325-z.

[43] P. Whittaker, D.R. Boughner, R. Kloner, Analysis of healing after myocardial infarction using polarized light microscopy, Am. J. Pathol. 134 (4) (1989) 879–893.

[44] X. Zhuan, X. Luo, H. Gao, R.W. Ogden, Coupled agent-based and hyperelastic modelling of the left ventricle post-myocardial infarction, Int. J. Numer. Methods Biomed. Eng. 35 (1) (2019) e3155, http://dx.doi.org/10.1002/cnm.3155.

[45] M. Nahrendorf, F. Wiesmann, K.-H. Hiller, K. Hu, C. Waller, J. Ruff, T.E. Lanz, S. Neubauer, A. Haase, G. Ertl, W.R. Bauer, Serial CINE-magnetic resonance imaging of left ventricular remodeling after myocardial infarction in rats, J. Magn. Reson. Imaging 14 (5) (2001) 547–555, http://dx.doi.org/10.1002/jmri.1218.

[46] V. Richard, C.E. Murry, K.A. Reimer, Healing of myocardial infarcts in dogs: effects of late reperfusion, Circulation 92 (7) (1995) 1891–1901, http://dx.doi.org/10.1161/01.CIR.92.7.1891.

[47] D.S. Fieno, H.B. Hillenbrand, W.G. Rehwald, K.R. Harris, R.S. Decker, M.A. Parker, F.J. Klocke, R.J. Kim, R.M. Judd, Infarct resorption, compensatory hypertrophy, and differing patterns of ventricular remodeling following myocardial infarctions of varying size, J. Am. Coll. Cardiol. 43 (11) (2004) 2124–2131, http://dx.doi.org/10.1016/j.jacc.2004.01.043.

[48] M. Fishbein, D. Maclean, P. Maroko, Experimental myocardial infarction in the rat: qualitative and quantitative changes during pathologic evolution, Am. J. Pathol. 90 (1) (1978) 57–70.

[49] H.B. Hillenbrand, J. Sandstede, S. Störk, B. Ramsayer, D. Hahn, G. Ertl, H. Koestler, W. Bauer, C. Ritter, Remodeling of the infarct territory in the time course of infarct healing in humans, Magn. Reson. Mater. Phys. Biology Med. 24 (2011) 277–284, http://dx.doi.org/10.1007/s10334-011-0262-y.

[50] L.H. Opie, P.J. Commerford, B.J. Gersh, M.A. Pfeffer, Controversies in ventricular remodelling, Lancet 367 (9507) (2006) 356–367, http://dx.doi.org/10.1016/S0140-6736(06)68074-4.

[51] J.S. Burchfield, M. Xie, J.A. Hill, Pathological ventricular remodeling: mechanisms: part 1 of 2, Circulation 128 (4) (2013) 388–400, http://dx.doi.org/10.1161/CIRCULATIONAHA.113.001878.

[52] L. Geerts-Ossevoort, P. Bovendeerd, F. Prinzen, T. Arts, K. Nicolay, Myofiber orientation in the normal and infarcted heart, assessed with MR-diffusion tensor imaging, in: Computers in Cardiology 2001. Vol. 28, IEEE, 2001, pp. 621–624, http://dx.doi.org/10.1109/CIC.2001.977732.

[53] C.O. Leong, C.N. Leong, Y.M. Liew, A. Al Abed, Y.F.A. Aziz, K.H. Chee, G.S. Sridhar, S. Dokos, E. Lim, The role of regional myocardial topography post-myocardial infarction on infarct extension, Int. J. Numer. Methods Biomed. Eng. 37 (8) (2021) e3501, http://dx.doi.org/10.1002/cnm.3501.

[54] A. Bailey, S. Bazin, T. Sims, M. Le Lous, C. Nicoletis, A. Delaunay, Characterization of the collagen of human hypertrophic and normal scars, Biochim. et Biophys. Acta (BBA)-Protein Struct. 405 (2) (1975) 412–421, http://dx.doi.org/10.1016/0005-2795(75)90106-3.

[55] I. Williams, K. McCullagh, I. Silver, The distribution of types I and III collagen and fibronectin in the healing equine tendon, Connect. Tissue Res. 12 (3–4) (1984) 211–227, http://dx.doi.org/10.3109/03008208409013684.

[56] M.T. Vivaldi, D.R. Eyre, R.A. Kloner, F.J. Schoen, Effects of methylprednisolone on collagen biosynthesis in healing acute myocardial infarction, Am. J. Cardiol. 60 (4) (1987) 424–425, http://dx.doi.org/10.1016/0002-9149(87)90277-3.

[57] I. Medugorac, Collagen type distribution in the mammalian left ventricle during growth and aging, Res. Exp. Med. 180 (3) (1982) 255–262, http://dx.doi.org/10.1007/BF01852298.

[58] J. Humphrey, R. Strumpf, F. Yin, Determination of a constitutive relation for passive myocardium: II.- parameter estimation, J. Biomech. Eng. 112 (1990) 333–346, http://dx.doi.org/10.1115/1.2891194.

[59] H. Ghaemi, K. Behdinan, A. Spence, In vitro technique in estimation of passive mechanical properties of bovine heart: Part I. Experimental techniques and data, Med. Eng. Phys. 31 (1) (2009) 76–82, http://dx.doi.org/10.1016/j.medengphy.2008.04.008.

[60] F. Ahmad, S. Soe, J. Albon, R. Errington, P. Theobald, Quantifying the microstructural and biomechanical changes in the porcine ventricles during growth and remodelling, Acta Biomater. 171 (2023) 166–192, http://dx.doi.org/10.1016/j.actbio.2023.09.044.

[61] J.C. Forrester, B.H. Zederfeldt, T.L. Hayes, T.K. Hunt, Wolff's law in relation to the healing skin wound, J. Trauma Acute Care Surg. 10 (9) (1970) 770–779.

[62] C. Frank, B. MacFarlane, P. Edwards, R. Rangayyan, Z.-Q. Liu, S. Walsh, R. Bray, A quantitative analysis of matrix alignment in ligament scars: a comparison of movement versus immobilization in an immature rabbit model, J. Orthop. Res. 9 (2) (1991) 219–227, http://dx.doi.org/10.1002/jor.1100090210.

[63] P.P. Provenzano, D.A. Martinez, R.E. Grindeland, K.W. Dwyer, J. Turner, A.C. Vailas, R. Vanderby Jr., Hindlimb unloading alters ligament healing, J. Appl. Physiol. 94 (1) (2003) 314–324, http://dx.doi.org/10.1152/japplphysiol.00340.2002.

[64] F.C. Yin, R.K. Strumpf, P.H. Chew, S.L. Zeger, Quantification of the mechanical properties of noncontracting canine myocardium under simultaneous biaxial loading, J. Biomech. 20 (6) (1987) 577–589, http://dx.doi.org/10.1016/0021-9290(87)90279-X.

[65] K.L. Billiar, M.S. Sacks, Biaxial mechanical properties of the natural and glutaraldehyde treated aortic valve cusp, part I: experimental results, J. Biomech. Eng. 122 (1) (2000) 23–30, http://dx.doi.org/10.1115/1.429624.

[66] K.L. Billiar, M.S. Sacks, Biaxial mechanical properties of the native and glutaraldehyde-treated aortic valve cusp, part II: a structural constitutive model, J. Biomech. Eng. 122 (4) (2000) 327–335, http://dx.doi.org/10.1115/1.1287158.

[67] K.D. Costa, J.W. Holmes, A.D. McCulloch, Modelling cardiac mechanical properties in three dimensions, Philos. Trans. R. Soc. Lond. Ser. A Math. Phys. Eng. Sci. 359 (1783) (2001) 1233–1250, http://dx.doi.org/10.1098/rsta.2001.0828.

[68] H. Gao, W. Li, L. Cai, C. Berry, X. Luo, Parameter estimation in a Holzapfel–Ogden law for healthy myocardium, J. Engrg. Math. 95 (2015) 231–248, http://dx.doi.org/10.1007/s10665-014-9740-3.